



ANNUAL
REVIEWS **Further**

Click [here](#) to view this article's online features:

- Download figures as PPT slides
- Navigate linked references
- Download citations
- Explore related articles
- Search keywords

Shared Molecular Mechanisms of Membrane Transporters

David Drew¹ and Olga Boudker²

¹Centre for Biomembrane Research, Department of Biochemistry and Biophysics, Stockholm University, SE-106 91 Stockholm, Sweden; email: ddrew@dbb.su.se

²Department of Physiology and Biophysics, Weill Cornell Medical College, New York, NY 10065; email: olb2003@med.cornell.edu

Annu. Rev. Biochem. 2016. 85:543–72

First published online as a Review in Advance on March 21, 2016

The *Annual Review of Biochemistry* is online at biochem.annualreviews.org

This article's doi:
10.1146/annurev-biochem-060815-014520

Copyright © 2016 by Annual Reviews.
All rights reserved

Keywords

alternating-access mechanisms, membrane proteins, secondary transporters, structural dynamics, elevator model, rocking-bundle model

Abstract

The determination of the crystal structures of small-molecule transporters has shed light on the conformational changes that take place during structural isomerization from outward- to inward-facing states. Rather than using a simple rocking movement of two bundles around a central substrate-binding site, it has become clear that even the most simplistic transporters utilize rearrangements of nonrigid bodies. In the most dramatic cases, one bundle is fixed while the other, structurally divergent, bundle carries the substrate some 18 Å across the membrane, which in this review is termed an elevator alternating-access mechanism. Here, we compare and contrast rocker-switch, rocking-bundle, and elevator alternating-access mechanisms to highlight shared features and novel refinements to the basic alternating-access model.

Contents

INTRODUCTION	544
MEMBRANE TRANSPORTERS: THE BASICS	544
THE ALTERNATING-ACCESS MECHANISM	545
THE ROCKER-SWITCH MODEL	547
Symmetric Minimal Rocker-Switch Mechanism	547
Evolution of the Rocker-Switch Mechanism for Asymmetric Transport	549
Structural and Functional Asymmetry in Major Facilitator Superfamily Transporters	549
The Coupling of Gating Helices and Global Rocker-Switch Rearrangements	552
Summary of the Rocker-Switch Mechanism	553
THE ROCKING-BUNDLE MODEL	553
The Rocking-Bundle Model of LeuT Fold Transporters	553
Diversity in Local Gating and Global Rocking-Bundle Movements	555
Comparison of the Rocker-Switch and Rocking-Bundle Models	556
THE ELEVATOR MODEL	557
The Architecture of Elevator Transporters	557
Extreme Asymmetry of Domains in Elevator-Like Transporters	562
Substrate Binding and Gating	563
CONCLUSIONS AND FUTURE PERSPECTIVES	564
The Dynamics of Structural Transitions	564
Summary	565

INTRODUCTION

Membrane transporters mediate either the passive or active transport of solutes ranging from ions to nutrients to signaling molecules and drugs. The alternating-access model is a conceptual mechanism, proposed in the mid-1950s (1–3), that explains their mode of action. The linchpin of the mechanism is the conformational transition of the transporter between states in which the substrate-binding site is exposed to opposite sides of the membrane in an alternating fashion. During the past decade, understanding of the molecular mechanisms of transporters has grown dramatically, with the crystal structures of transporters belonging to different families having been captured in multiple functional states. By combining these crystal structures with biophysical and computational approaches, a clearer understanding of the different ways in which the substrate can be transported is emerging. In this review, we describe novel, conceptual refinements to the basic alternating-access model.

MEMBRANE TRANSPORTERS: THE BASICS

In passive transporters—also called uniporters, facilitators, or equilibrative transporters—conformational transitions between outward- and inward-facing states occur stochastically and spontaneously, facilitating substrate equilibration across both sides of the membrane. These structural transitions are thought to occur via additional intermediate occluded states, whereby access to the binding site from either side of the membrane is obstructed by a protein mass. Energetically, passive transporters resemble channels: The direction of substrate flow is determined only by its

electrochemical potential. Passive transporters differ from channels inasmuch as only a single substrate molecule is transported during each cycle of structural transitions. In contrast, in channels the diffusion of multiple substrates takes place upon channel opening through a relatively rigid, single conformation.

Secondary active transporters concentrate their substrates on one side of a membrane by coupling their movements to the symport or antiport of another solute or solutes (most typically ions), which themselves are moving thermodynamically downhill along their electrochemical potentials. Depending on whether driving solutes and substrates are moving in the same or opposite directions, these transporters are called, respectively, symporters or antiporters (exchangers). They are termed secondary active transporters because they utilize preexisting gradients of driving solutes as a source of energy; an independent source of energy is required to establish these gradients of driving solutes.

Secondary active transporters are conceptually and mechanistically similar to passive transporters. They are expected to be fully thermodynamically reversible, and the directionality of substrate flux is determined only by the combined electrochemical potentials of the substrate and the driving solute (or solutes). Indeed, closely related transporters are known to mediate either passive or active transport. Also, the identity of the driving solutes and coupling stoichiometry (i.e., how many molecules are transported per substrate) may vary. For instance, the major facilitator superfamily (MFS) of transporters includes members that mediate either the equilibrative or ion-dependent transport of sugars, with the latter being driven by the symport of either protons or sodium ions (4, 5).

The key energetic aspect of symport is that neither the substrate nor the driving ions are transported alone: They are only transported together. Such coupling can be established during binding, substrate-translocation steps, or both. For example, the binding of substrate and driving solute can be cooperative such that neither of them binds efficiently alone. Conversely, even if the binding of each solute occurs independently, the binding of both could be required for rapid structural isomerization. Similarly, coupled antiport processes can be established by making binding of the counter-transported solute a requirement for substrate release, for returning the transporter to its starting conformation, or for both.

THE ALTERNATING-ACCESS MECHANISM

Regardless of the source of energy, the linchpin of the transport mechanism is that the substrate-binding site is made accessible from one side of the membrane or the other (**Figure 1**). Such alternating accessibility can be achieved only through an allosteric coupling of extracellular and intracellular gates in a transporter. Thus, it appears that global structural transitions are a necessary means of information transfer between the two sides of the transporter. Interestingly, chloride-proton exchangers (CICs) (6) were thought, until recently, to be an exception to this rule because transport seemed to be associated only with the local movements of side chains within a rigid protein scaffold (7–9). However, new data suggest that global structural transitions are also likely to be part of the CIC mechanism (10–12). It should be noted that small perturbations, such as mutations or the binding of small molecules, can turn some transporters into channels, presumably by stabilizing the states in which both the extracellular and intracellular gates are open (e.g., a double mutant of the *Escherichia coli* CIC transporter becomes a channel) (6, 13, 14). Indeed, some transporter families, such as the CIC family, contain both transporters and bona fide channels (15).

Crystal structures have shown that most transporters can be described as operating by either a rocker-switch or a rocking-bundle mechanism (**Figure 1a,b**). In transporters using these mechanisms, the substrate-binding site is located at the interface of two domains, approximately halfway

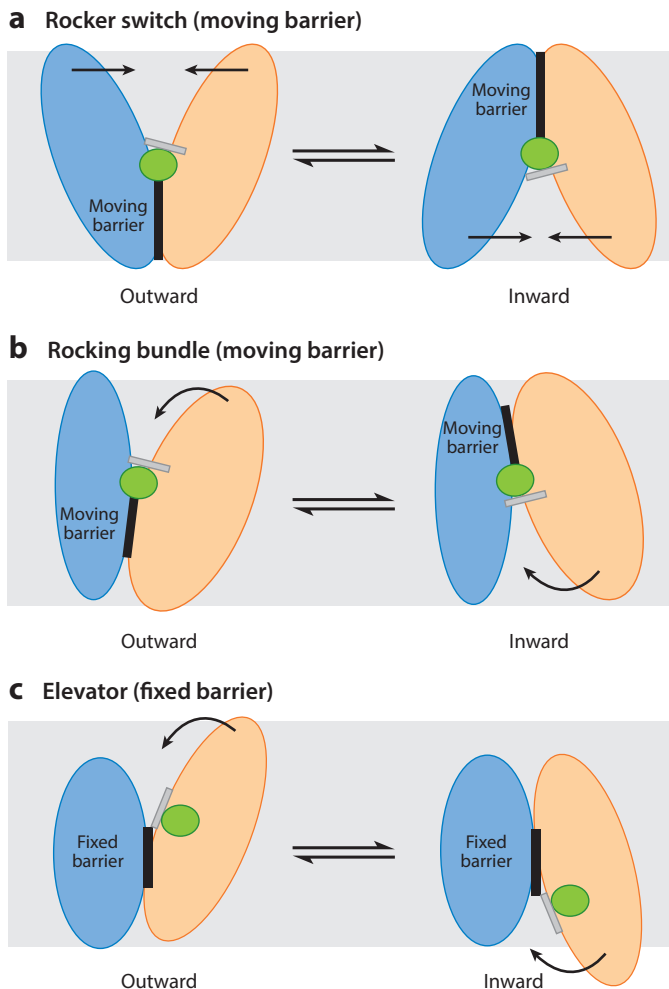


Figure 1

Alternating-access mechanisms. The major conformations of the moving-barrier alternating-access mechanism observed in (a) rocker-switch and (b) rocking-bundle proteins; for illustrative purposes, fully occluded intermediate conformations are not shown. In moving-barrier mechanisms, the substrate (*green sphere*) binds between two domains, catalyzing the rearrangement of the protein around the central substrate-binding site. In rocker-switch proteins, two structurally similar domains rock to afford alternating accessibility. In rocking-bundle proteins, one structurally dissimilar domain rearranges against a less labile domain to afford accessibility. Transport in rocker-switch and rocking-bundle proteins further involves local, substrate-induced gating rearrangements by helices located in either one or both of the domains (depicted here as a *thick line* over the substrate). In rocking-bundle proteins, the gates are more extensive than those in the rocker-switch mechanism; for this reason the rocking-bundle mechanism is also referred to as a gated-pore model. The relative contribution of global (rocking) and local (gating) rearrangements also varies among transporters that share a common architecture. (c) The fixed-barrier alternating-access mechanism observed in elevator proteins; for illustrative purposes, fully occluded intermediate conformations are not shown. In fixed-barrier mechanisms, the substrate (*green sphere*) binds to one of the domains, which moves against a structurally dissimilar immobile domain to physically translocate the substrate to the other side of a fixed barrier. As such, in elevator proteins, one domain moves against another relatively rigid domain to afford accessibility. Substrate binding and release in each state are likely facilitated by local gating transitions, primarily in the moving domain (gates are depicted here as a *thick line* over the substrate).

across the membrane. Basically, alternating access to the substrate-binding site is achieved when the barrier formed between the two domains on the cytoplasmic side of the membrane is moved apart and re-formed on the extracellular side. The realization of this transporter model is what Peter Mitchell (1, 1a) conceptualized as the moving-barrier mechanism. MFS transporters and those harboring the ubiquitous LeuT fold both use a moving-barrier mechanism (16, 17, 103) (**Figure 2a,b**).

More recently, a different type of alternating-access mechanism has emerged, the so-called elevator mechanism (**Figure 1c**). This mechanism was first seen in glutamate transporters (18) and later in sodium–proton exchangers (19) (**Figure 2c**). Elevator-like structural transitions have also been proposed for phosphorylation-coupled saccharide transporters (20), a structurally distinct phosphorylation-coupled vitamin C transporter (21), the sodium–dicarboxylate symporter vINDY (22, 23), and citrate transporter (24). Finally, several other transporters have architectural features highly suggestive of an elevator mechanism, including concentrative nucleoside transporters (25) and transporters of the AbgT family (26, 27). In the elevator alternating-access mechanism, the substrate-binding site is confined largely, or entirely, to a single domain that traverses the membrane along a relatively rigid, immobile scaffold domain. Thus, the barrier stays at a fixed position and the substrate moves across it, from the extracellular to the intracellular side. In reference to Mitchell's (1, 1a) moving-barrier model, we refer to the elevator model as a fixed-barrier mechanism (**Figure 1c**).

Although we do not discuss primary active adenosine triphosphate (ATP)-driven transporters in this review, it is interesting to note that they too show similar structural diversity and include transporters utilizing both rocker-switch and elevator-like mechanisms (28).

THE ROCKER-SWITCH MODEL

Symmetric Minimal Rocker-Switch Mechanism

The simplest version of a rocker-switch mechanism involves nearly symmetrical substrate binding and rigid-body movements of two symmetrically related bundles around a centrally located substrate-binding site (29, 30). In essence, the protein moves around the substrate, alternately exposing the binding site to each side of the membrane (31) (**Figure 1a**).

The transporters known as SWEETs (sugars will be exported transporters) are concentration-dependent sugar transporters in plants and animals (32). Bacterial homologs of sugar SWEET transporters, the so-called semi-SWEETs (33), seem to operate most closely to the definition of the rocker-switch mechanism (34–36) (**Figure 3a**). They are made up of only three transmembrane (TM) segments that come together to form parallel dimers in a membrane. Each bundle of three TM segments is oriented with its N- and C-termini facing, respectively, the extracellular or cytoplasmic solution (known as $N_{\text{out}}-C_{\text{in}}$ topology), as established by the positive-inside rule (37). The middle of TM1 in each bundle of three TM segments kinks outward at a highly conserved PQ-loop motif (38, 39) to form two helical parts, TM1a and TM1b (34–36). TM1a packs against TM2 in the symmetrically related bundle to seal the two bundles together. Structures of semi-SWEET sucrose transporters have been seen in outward-facing, occluded, and inward-facing conformations (34–36) (**Figure 3a**). The substrate-binding site is located between the two bundles, approximately halfway across the membrane (34–36). During the rocker-switch rearrangements, TM1a moves with the symmetrically related bundle, whereas TM1b moves with its own bundle (35). Although the density of sucrose bound in the occluded structures is not strong enough to unambiguously place the substrate, the best fit is for a sugar that is coordinated evenly by residues from both bundles (34, 36). The occluded conformation appears to be symmetric, with the substrate located in the central cavity and the two ends

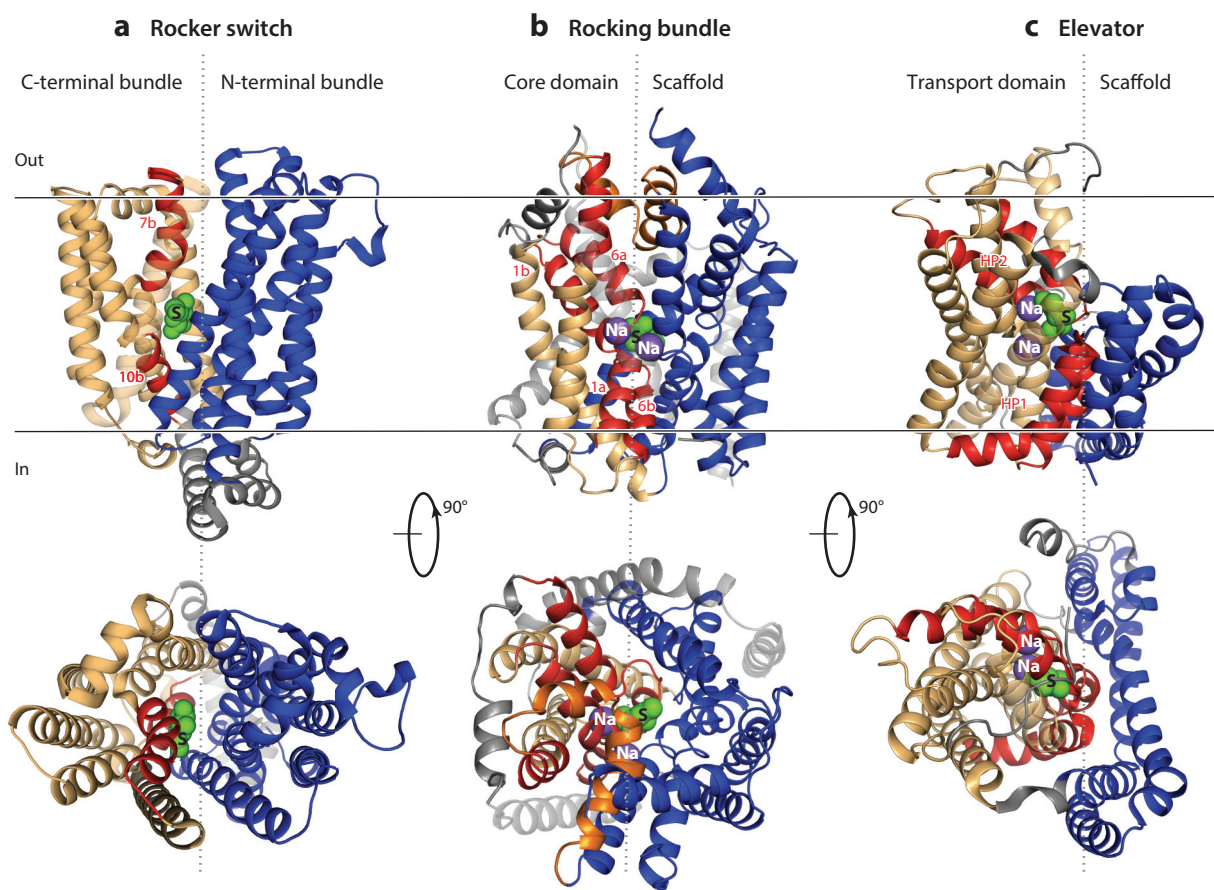


Figure 2

Representative transporter folds for different alternating-access mechanisms. (a) Rocker-switch proteins are made up of two helical bundles that are related by a pseudo-twofold symmetry axis that runs through the center of the transporter and perpendicular to the membrane plane, as shown for a major facilitator superfamily (MFS) fold transporter. In the MFS fold, each structurally similar bundle is made up of six transmembrane (TM) segments (N-terminal bundle TM segments are *blue*; C-terminal bundle TM segments are *red* and *light orange*) that are connected by a cytosolic loop. In this example of the sugar porter GLUT3 [Protein Data Bank (PDB) identification number 4ZW9], the substrate (*green spheres*) binds predominantly to the C-terminal bundle, whereby the discontinuous helices 7b and 10b form substrate-induced gates (*red*). (b) Rocking-bundle proteins are made up of intertwined, pseudo-symmetric repeats with inverted topology and an axis of symmetry parallel to the membrane plane, as shown for a LeuT fold transporter (PDB identification number 2A65). In this example of the amino acid transporter LeuT, the structurally distinct bundles are referred to as the scaffold domain (*blue*) and core domain (*red* and *light orange*). Substrate (*green spheres*) and sodium ions (*purple spheres*) are coordinated between the scaffold and the core domains. Elements of discontinuous helices form the extracellular (TM1b, 6a, and 7) and intracellular (TM1a) gates (*red*). (c) Elevator proteins are also typically made up of intertwined, pseudo-symmetric repeats with inverted topology and an axis of symmetry parallel to the membrane plane, as shown for the glutamate transporter homolog Glt_{Ph}. In this example of Glt_{Ph} (PDB identification number 2NWL), the structurally distinct bundles are referred to as the scaffold domain (*blue*) and transport domain (*red* and *light orange*). The scaffold domain (*blue*) is typically involved in oligomerization and is thinner than the transport domain (*red* and *orange*). Substrate (*green spheres*) and sodium ions (*purple spheres*) are bound solely within the transport domain. The tips of the helical hairpins (HP1 and HP2) form the extracellular and intracellular gates (*red*). Note that one or more helices in each of the representative folds have been rendered transparent to make it easier to illustrate features of the ion and/or substrate binding sites.

closed off via interactions between loops of the three-TM-segment bundles (36). As such, the V-like structure of the outward-facing conformation is first converted into an O-like structure in the occluded conformation before transitioning to the Λ -like structure of the inward-facing conformation (34–36) (**Figure 3a**). Thus, even in these minimalistic transporters, it is clear that the two bundles must bend and utilize rearrangements of nonrigid bodies.

Evolution of the Rocker-Switch Mechanism for Asymmetric Transport

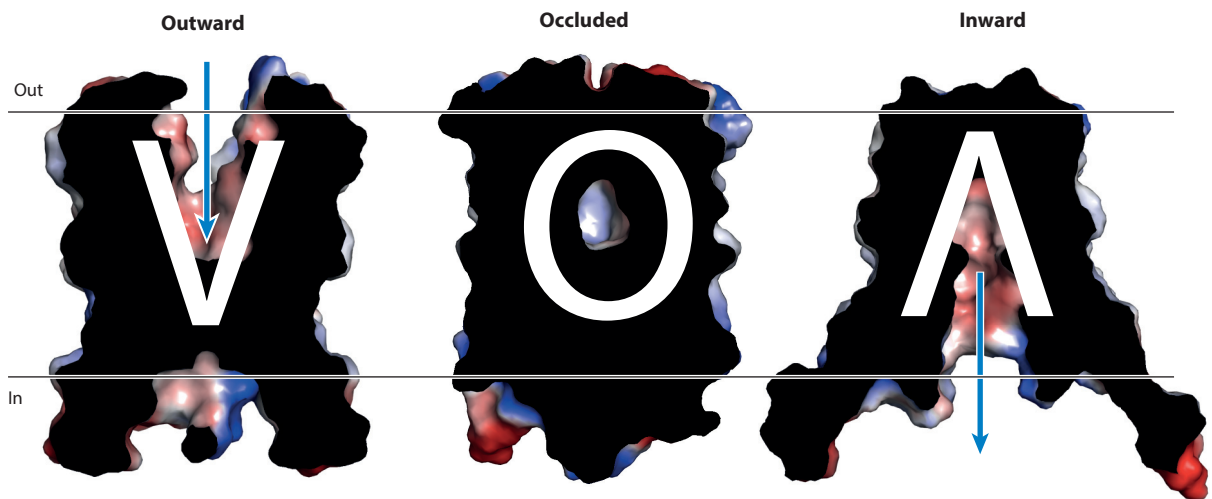
The small multidrug resistance (SMR) efflux transporter EmrE (from *E. coli*) exchanges two protons for one drug molecule using a single-site antiport mechanism (40). EmrE consists of four TM segments that, because they have no charge bias, insert with both an N_{out}-C_{out} and an N_{in}-C_{in} (dual) topology (41–43). However, unlike the semi-SWEETs, there is no segment exchange between bundles. As such, interbundle interactions are poor and, indeed, parallel EmrE dimers have also been observed in membranes, leading to much debate regarding the correct topology (43, 45). Based on the available crystal structures (46, 47), and fluorescence resonance energy transfer (FRET) and nuclear magnetic resonance studies (44), an antiparallel EmrE dimer is thought to be the predominant functional form, with the substrate-binding site located at the protomer interface. A rocker-switch model based on identical V-like outward- and inward-facing EmrE structures has been proposed, but an occluded state has not yet been identified (44, 46, 47). In contrast to the semi-SWEETs, which have narrow substrate specificity for fairly symmetric sugar molecules, EmrE has broader substrate specificity and is also capable of transporting asymmetric, organic cation molecules. We speculate that the selective pressure on EmrE to evolve an antiparallel orientation may have occurred to place equivalent residues from two polypeptide chains in different positions around the substrate-binding site in order to recognize asymmetric compounds, for example, ethidium bromide (48). Interestingly, the bacterial vitamin B3 transporter PnuC has the same fold as the full-length eukaryotic SWEET proteins, with the three-TM-segment repeats fused to form a 3 + 1 + 3 topology (49). Unlike the SWEETs, the three-TM-segment repeats in PnuC share low sequence similarity with one another and most of the pseudosymmetry-related residues use different side chain chemistry to coordinate the asymmetric substrate nicotinamide riboside (49). Thus, the antiparallel insertion of structural repeats, gene duplication, and fusion might be the result of two, potentially complementary, evolutionary mechanisms for developing specificity for diverse, asymmetric substrates.

Structural and Functional Asymmetry in Major Facilitator Superfamily Transporters

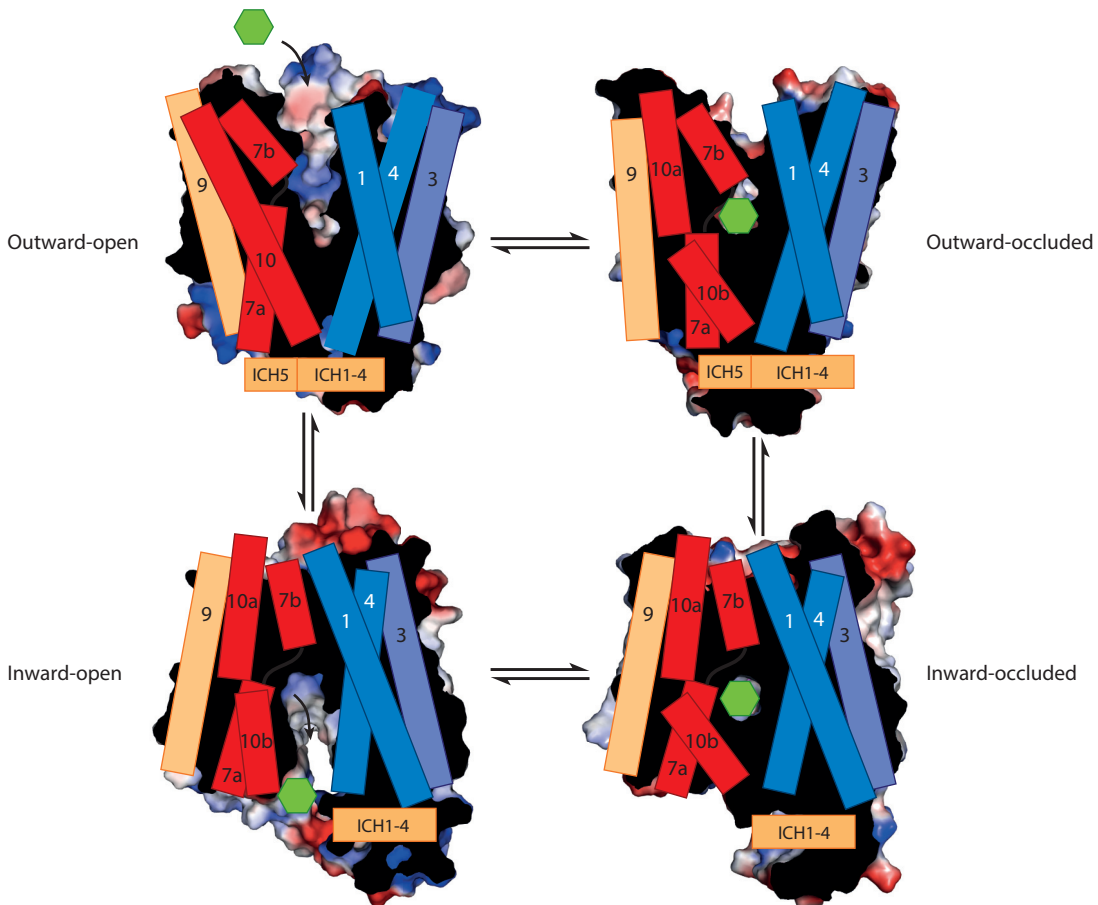
Dimeric semi-SWEETs and SMR proteins demonstrate features of ancestral transporters, illustrating how they may have evolved through gene duplication, divergence, and fusion to lead to the frequent occurrence of pseudosymmetric motifs with inverted topology in modern, larger transporters (41, 43–50). MFS transporters, which show these typical features, are the largest superfamily of secondary active transporters (51). The MFS fold consists of 12 TM segments that are made up of two symmetrically related bundles of six TM segments that are connected by a cytosolic loop (4, 52, 57), which is sometimes ordered, such as in the MFS subfamily of sugar porters (53, 54) (**Figure 2a**). The six-TM-segment bundles are often referred to as the N- and C-terminal TM bundles, and they are themselves made up of two structurally inverted repeats of three TM segments (55).

The first crystal structures describing the MFS fold were those of the lactose-H⁺ symporter LacY and the glycerol-3-phosphate-phosphate antiporter GlpT (4, 57). Since then, the structures of MFS transporters that recognize sugars (5, 54, 58–62), oligopeptides (63–67), nitrate (68–72), phosphate (73), and xenobiotics (74, 75) have been determined in one or several distinct

a Semi-SWEET rocker-switch mechanism



b Glucose (GLUT) transporter rocker-switch mechanism



conformations. The symmetrically related bundles of six TM segments form the characteristic V- and Λ -like structures in, respectively, the outward- and inward-facing conformations (16, 29) (**Figure 3b**). However, unlike the SWEETs they do not seem to readily form a symmetrically occluded O-like conformation (29), with perhaps the exceptions of the multidrug H⁺ antiporter EmrD (74) and the oxalate antiporter OxIT (76). Instead, in most occluded MFS structures the cavity still has a clear orientation preference, and states are typically referred to as outward-occluded or inward-occluded conformations (16, 29) (**Figure 3b**).

The vitamin B3 transporter PnuC and the facilitative glucose transporter GLUT3 are two representative proteins from the SWEETs and the MFS fold for which the substrate could be confidently fitted into the electron density of the occluded structures (49, 60). In PnuC, residues in each of the three-TM-segment bundles evenly coordinate the bound nicotinamide riboside (49). In contrast, in the outward-occluded structure of GLUT3, almost all of the extensive interactions with the bound sugar are from residues located on the C-terminal TM bundle, and only one residue in the N-terminal TM bundle contributes to the binding site (60). Thus, PnuC binds its substrate symmetrically, and its occluded conformation has a symmetric O-like shape (49), but GLUT3 binds its substrate asymmetrically and shows an asymmetric outward-occluded conformation (60). The binding mode seen in GLUT3 is consistent with the mode seen in the sugar-bound GLUT1 and the related *E. coli* D-xylose-H⁺ symporter homolog XylE structures (53, 54). In unrelated oligopeptide, nitrate, and phosphate MFS transporters, residues on the C-terminal TM bundle also seem to account for most of the interactions with the bound substrate (65, 66, 71, 73, 77).

By comparing the outward-open and outward-occluded conformations of GLUT3 it has been shown that the asymmetric occlusion is due to an inward bending in the half-helix TM7b, which is located on the C-terminal TM bundle (60) (**Figure 3b**). TM7b stabilizes the occluded conformation through a conserved asparagine (Asn286), which has moved inward to coordinate the bound sugar (60). The neighboring bulky tyrosine residues Tyr290 and Tyr291 form the substrate-induced occlusion, although they do not have any direct interaction with the sugar molecule. In the outward-occluded structure of *E. coli* XylE, an equivalently placed tyrosine residue (Tyr298) was likewise found to form the outside occlusion (53). By comparing the structures of sugar porters crystallized in the inward-occluded and inward-open conformations, it has been shown that the asymmetric occlusion on the inside is mostly formed by the half-helix TM10b (59, 61, 78) (**Figure 3b**).

Figure 3

Rocker-switch alternating-access mechanisms for the sugar transporters known as semi-SWEETs (sugars will eventually be exported transporters) and sugar porter transporters belonging to the major facilitator superfamily (MFS). (a) Slab through the surface electrostatic potential of the outward [*left*; Protein Data Bank (PDB) identification number 4X5N], occluded [*middle*; PDB identification number 4RNG], and inward-facing [*right*; PDB identification number 4X5M] bacterial semi-SWEET structures, as viewed within the plane of the membrane. The surfaces highlight the substrate translocation pathway through the center of the protein, where access is controlled by a rocker-switch mechanism. The rocker-switch transport mechanism can also be demonstrated by bringing your two hands together at the wrists to form a V shape for the outward conformation. Next, bringing the tips of your fingers together forms the occluded conformation. Opening your wrists while keeping your fingers together to form a Λ shape shows the inward-facing conformation. (b) Slab through the surface electrostatic potential of the outward-open [*top left*; PDB identification number 4YBQ], outward-occluded [*top right*; PDB identification number 4GBZ], inward-occluded [*bottom right*; PDB identification number 4JA4], and inward-open [*bottom left*; PDB identification number 4YB9] sugar porter structures. Overlaid is the schematic representation of the rocker-switch movement of the N-terminal [*blue* and *purple*] and C-terminal [*red* and *light orange*] transmembrane (TM) segment bundles. Further local gating conformational changes discontinuous helices TM 7b and 10b [*red*] occlude the substrate from, respectively, the outside and inside. In addition to the intracellular salt-bridge network (see sidebar, Salt Bridges in Monosaccharide Sugar Porters), intracellular helices (ICH1-5; *light orange*) also contribute to stabilizing the outward-facing conformation. Panel *b* is adapted with permission from Reference 78.

TMs 7 and 10 are related by an inverted pseudosymmetry and have consistently been found to account for the largest fraction of the substrate-binding site in sugar porter proteins (53, 54, 60), which is in agreement with previous functional data (79–81). Comparisons of the structures of oligopeptide and nitrate transporters in both inward-occluded and inward-open conformations have likewise shown that a local rearrangement of TM10 and the adjoining TM11 are required for substrate release (16, 64, 72). Thus, in many MFS transporters the C-terminal TM bundle has the critical role in substrate binding and occlusion. However, in others, such as LacY, TMs 1 and 4 in the N-terminal TM bundle seem to be more extensively involved (82, 83).

Taken together, TMs 1 and 4 in the N-terminal TM bundle and TMs 7 and 10 in the C-terminal TM bundle are positioned in the center of the transporter, and they account for the majority of the substrate binding and occlusion formed in MFS transporters (16) (**Figure 3b**). Importantly, TMs 1, 4, 7, and 10 are the first TM segments in each of the three-TM-segment repeats. Moreover, those TM segments that undergo local, asymmetric rearrangements upon substrate binding in a particular MFS transporter are often discontinuous helices—i.e., they contain an unwound region. Due to their central role in substrate binding and occlusion formation, TMs 1, 4, 7, and 10 have also been described as gating helices (84, 85).

The Coupling of Gating Helices and Global Rocker-Switch Rearrangements

The key aspect of the alternating-access mechanism is that it prohibits simultaneous access from both sides of the membrane to the substrate-binding site. In MFS transporters cavity-closing contacts are predominantly formed between TMs 1 and 7 on the outside and between TMs 4 and 10 on the inside (16, 29). Therefore, substrate binding induces the local movement of gating helices that eventually come together to close off the cavity during global rocker-switch isomerization (**Figure 3b**). Thus, we think that the local binding-site occlusion on one side of the membrane is a structural prerequisite to the rocker-switch transition that opens access to the opposite side. If so, one would expect substrate binding and coordination to favor rocker-switch isomerization. Indeed, the kinetics of the glucose transporter GLUT1 have been studied since the 1950s, and it is well known that the addition of cold sugar to the inside increases the uptake of radioactively labeled hot sugar added to the outside—i.e., so-called *trans* acceleration (86). Consistently, after substrate release into the cytoplasm, the outward transition of the unloaded GLUT1 transporter is the slowest step of the transport cycle (86, 87).

The central role of the substrate in catalyzing rocker-switch isomerization has also been demonstrated in LacY, where equilibrium substrate exchange and counterflow are unaffected by the imposition of a proton motive force (31, 88–90). What is the nature of the energetic barrier that is lowered by substrate binding? After the crystal structures of LacY and GlpT were determined, it was proposed that this barrier involves the breakage and re-formation of salt bridges that hold the N- and C-terminal bundles together (4, 57, 91, 92). Indeed, interbundle salt bridges have consistently been found in MFS transporters and are often proximal to the central cavity (5, 63, 64, 73, 93). In the melibiose transporter MelB they are referred to as ionic-lock interactions (5). Although it is not clear in all cases how substrate binding is coupled to the disruption of these ionic interactions, it is notable that in H⁺-coupled MFS transporters the protonation state of residues forming the interbundle salt bridges are often linked to substrate binding (29, 91, 94). Interestingly, in the subfamily of sugar porters, interbundle salt bridges are formed only on the cytoplasmic side, stabilizing the outward-facing conformation (see sidebar, Salt Bridges in Monosaccharide Sugar Porters). In the sugar porter proteins the gating helix TM10b is part of a strictly conserved, cytosolic interbundle salt-bridge network. Crystal structures show that when TM7b moves inward to coordinate the sugar, it no longer interacts tightly with TM10, thus presumably facilitating TM10b

SALT BRIDGES IN MONOSACCHARIDE SUGAR PORTERS

In GLUT transporters no salt bridges are observed near the central cavity, in either outward- or inward-facing conformations (54, 60, 78), perhaps to avoid inadvertent proton coupling. Instead, interbundle salt bridges are formed far from the central cavity and only in the outward-facing conformation, linking the cytoplasmic ends of TMs 3, 4, and 5 in the N-terminal transmembrane (TM) bundle to those of TMs 9, 10, and 11 in the C-terminal TM bundle (60, 78). Highlighting their importance, these charged residues are the most highly conserved from bacteria to man, and they make up well-described sugar porter signature motifs (51, 97). The charged residues are also structurally related by a pseudo-twofold symmetry axis that runs through the center of the transporter and perpendicular to the membrane plane (78). In the inward-facing conformation, the interbundle salt bridges are broken and are located far apart, as first predicted for the bacterial homolog Xyle (59). In the inward-facing conformation, no interbundle salt bridges are formed on the extracellular side. Consistently, the substitution of the salt-bridge-forming residues with neutral amino acids arrests GLUT transporters in an inward-facing conformation (98).

movement and salt-bridge breakage (78). The physical coupling between gating helices 7 and 10 in sugar porter transporters is clearly supported biochemically (78, 95, 96). Thus, salt-bridge breakage appears to be coupled to substrate binding, either indirectly or directly, in both proton-coupled and facilitative MFS transporters.

Summary of the Rocker-Switch Mechanism

The V-shaped architecture formed by two structurally similar bundles is a characteristic feature of rocker-switch proteins (**Figure 2a** and **Figure 3**). Multidrug MATE transporters meet this criterion, and it has been proposed that they also utilize a rocker-switch mechanism; however, only structures in the outward-facing conformation have been determined (99–102). As outlined here, in rocker-switch proteins the two bundles do not move solely as rigid bodies during the transport cycle (64, 73). Furthermore, as highlighted by the MFS transporters, substrate binding can be asymmetric to varying degrees and can be accompanied by local asymmetric rearrangements of discontinuous TM segments (**Figure 3b**). These local gating movements are coupled to global rocker-switch transitions by mechanisms that are only just beginning to be understood.

THE ROCKING-BUNDLE MODEL

The Rocking-Bundle Model of LeuT Fold Transporters

In the rocking-bundle alternating-access mechanism, substrate binding between two structurally distinct domains catalyzes the coupled movement of outside and inside gates around a centrally located substrate-binding site (17) (**Figure 1b**). The amino acid–sodium symporter LeuT, a neurotransmitter–sodium symporter (NSS) homolog from *Aquifex aeolicus*, is a prototypical example of a transporter with a rocking-bundle alternating-access mechanism (103) (**Figure 2b**). Unexpectedly, it was found that the LeuT fold is common, and many different transporter families share the same architecture (103–109). The LeuT fold is made up of two structurally inverted repeats of five TM segments (TMs 1–5 and TMs 6–10) that intertwine to form two structurally distinct bundles (17, 103). The pseudo-twofold symmetry axis runs through the center of the transporter but, unlike in the rocker-switch proteins, is parallel to the membrane plane (17, 50,

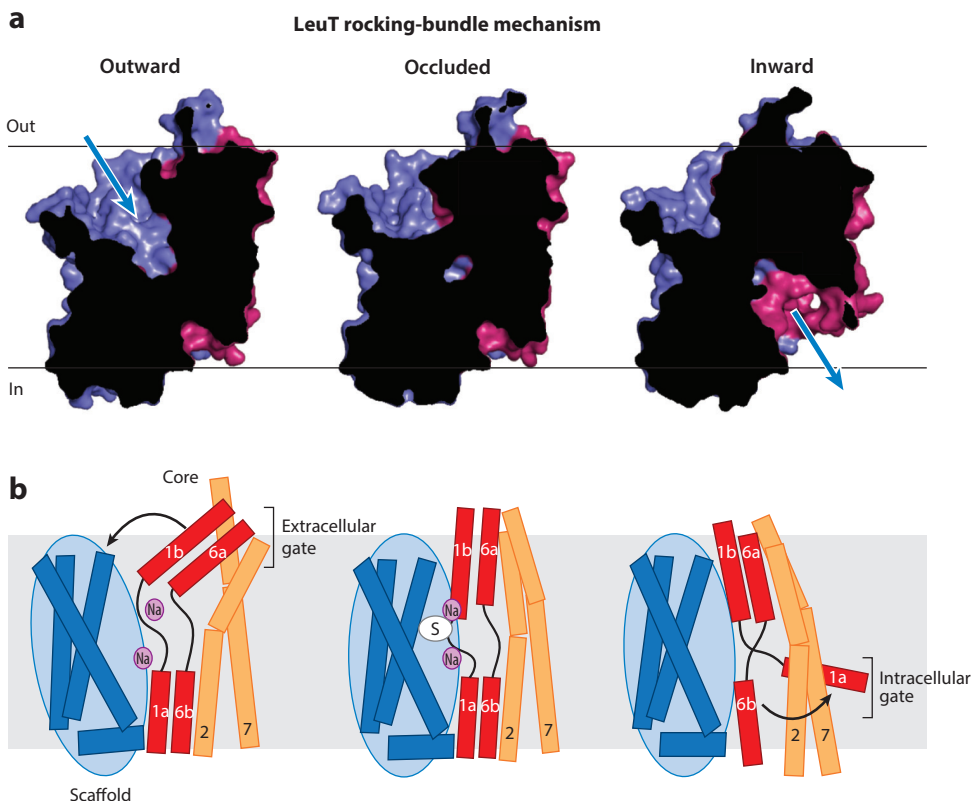


Figure 4

Rocking-bundle alternating-access mechanism for the sodium-coupled amino acid symporter LeuT. (a) Slab through the surface of the outward-open (left; Protein Data Bank (PDB) identification number 3TT1), outward-occluded (middle; PDB identification number 2A65), and inward-open (right; PDB identification number 3TT3) bacterial LeuT structures, as viewed within the plane of the membrane. The surfaces of the scaffold (purple) and core (magenta) domains highlight the substrate translocation pathway, which is on an angle through the protein and for which access is controlled by a rocking-bundle alternating-access mechanism. (b) Schematic representation of the rocking-bundle-type rearrangement of the core domain (red and light orange) against the scaffold domain (blue). Further local conformational changes of the extracellular TMs 1b, 6a (red), and 7 (light orange), and intracellular TM1a define, respectively, the outside and inside gates. The two sodium ions, Na1 and Na2, are shown as magenta spheres, and the substrate is shown as a white oval. Panel b is adapted with permission from Reference 110.

103) (Figure 3a and Figure 4a). As for MFS proteins, LeuT fold crystal structures have revealed outward- and inward-facing open and occluded structures, as well as fully occluded intermediate states (110, 111). In the LeuT fold, the two distinct bundles are referred to as the scaffold domain (TM3 and TM4, and TM8 and TM9) and the core domain (TM1 and TM2, and TM6 and TM7) (103) (Figure 2b and Figure 4b). The scaffold and core domains are linked by the helices TM5 and TM10. The core domain is characterized by two antiparallel, discontinuous helices, TM1 and TM6, which make up a large fraction of the substrate and, for ion-coupled members, ion-binding sites (103, 110, 111). The scaffold domain is formed by two overlapping V-shaped helical motifs. In LeuT, the outward-open conformation is stabilized by sodium binding, as

revealed by site-directed spin labeling and electron paramagnetic resonance (EPR) analysis (112). One Na⁺ ion binds the unwound region of TM1 in the core domain and TM8 in the scaffold domain (103). This sodium site (Na2) is conserved in all Na⁺-dependent LeuT fold transporters (103, 113–115). Another, nonconserved site (Na1) is confined to the core domain and is formed by side chains of residues on TMs 1b, 6a, and 7, and by the substrate amino acid (103).

The extracellular core TM segments 1b, 6a, and 7 move toward the scaffold TM segments 3 and 8 to provide occlusion of the coordinated substrate (103, 116, 117) (**Figure 4b**). The tight packing of the core against the scaffold domain via extracellular loop 4 (between TM segments 7 and 8) closes the outside cavity. These structural events seem to precede the rocking movement of the core bundle that leads to an inward-occluded conformation. In MFS transporters, interbundle salt bridges need to be broken, and sometimes re-formed, to facilitate global rearrangements (91, 92). In LeuT there is also an important evolutionarily conserved salt bridge that forms during gating on the extracellular side (116, 118). The breaking and re-forming of ionic interactions between residues in the cytoplasmic regions of TM1 and scaffold TM8 also are thought to be key to the function of NSS transporters (119). Between the inward-occluded and the inward-open conformation, the intracellular gate of TM1a moves significantly outward to enable cytosolic release of substrate (116) (**Figure 4b**). Molecular dynamic simulations of the LeuT fold transporters LeuT, Mhp1, and vSGLT support the idea of allosteric coupling occurring between the intracellular release of sodium and substrate (114, 115, 120). Likewise, crystal structures of the LeuT fold transporter MhsT have shown that sodium in the Na2 site is more poorly coordinated in the occluded conformation due to increased water solvation, which is facilitated by a local unwinding in the linker helix TM5 (121). Furthermore, extensive crystal structures of the LeuT fold member BetP, which have been captured in all the major conformations, show precisely how the coordination of sodium at the Na2 site changes during the transport cycle to set up substrate binding and dissociation (113).

Diversity in Local Gating and Global Rocking-Bundle Movements

Interestingly, there is substantial variation in LeuT fold transporters in terms of which of the two structural domains moves the most and by how much. The substrate-dependent local gating transitions also vary. For instance, in the hydantoin–sodium symporter Mhp1, sodium binds only at the Na2 site but not at the Na1 site (104, 114). Consequently, substrate binding induces the extracellular gating movements that are different from those described for LeuT, and it involves the end of TM 10 and the preceding loop, which packs over the substrate (104, 114, 122). Moreover, in Mhp1 the scaffold (referred to as a hash domain) is mobile and rocks around the core bundle, which remains stationary in the membrane. The movements of the flexible linker TM5, rather than TM1a, facilitate substrate release (114). Another example of mechanistic diversity is demonstrated by the conformational changes seen in the betaine–sodium symporter BetP. It is a trimer, held together primarily by the packing of an amphipathic helix and an N-terminal helix (not part of the five-TM repeat) (105, 113). This trimerization mode of BetP likely restricts the mobility of the core domain, and its global rearrangements are smaller and more symmetric compared with those seen in either LeuT or Mhp1 (104, 105, 113, 114). Additionally, the extracellular gate is different from either Mhp1 or LeuT (105, 113). Again, this might be a consequence of Na⁺ ion binding at a different location from the Na1 site in LeuT; interestingly, the site is at the interface between scaffold and core TM helices, similar to Na2 (105, 113).

Transporters with LeuT fold vary significantly in the types of substrates transported and in the identity of the driving solutes. Additionally, many of the transporters belonging to this

superfamily possess secondary substrate-binding sites located either in the extracellular or intracellular vestibules (120, 123). These sites may play regulatory roles or serve as transient binding sites along the substrate translocation pathway. In LeuT, both substrates and noncompetitive inhibitors bind at the same site, which is located more extracellularly compared with the primary substrate binding site (reviewed in 123).

Crystal structures of $\text{Na}^+(\text{H}^+)\text{-Ca}^{2+}$ exchangers in outward- and inward-facing conformations have shown that they, like LeuT fold transporters, are also made up of two structurally inverted repeats of five TM segments that come together to form two distinct bundles, referred to as gate and core domains (124, 125, 125a). It has been proposed that the gate domain, which is made of TM1 and TM6, rocks around the eight-TM-segment ion-binding core domain. In addition, a local outward movement of the half-helix TM2a in the core domain underlies intracellular Ca^{2+} release, which bears a resemblance to the TM1a movement described in LeuT.

Overall, the rocking-bundle proteins are composed of two structurally distinct bundles, with one domain predominantly rocking around the other (**Figure 1b**). The uracil transporter UraA and the structurally related transporters of the solute carrier SLC26/SulP family also fit this generalized description, and they show considerable architectural similarity to $\text{Na}^+(\text{H}^+)\text{-Ca}^{2+}$ exchangers (126, 127).

Comparison of the Rocker-Switch and Rocking-Bundle Models

Rocking-bundle and rocker-switch transporters share considerable similarities (**Figure 1a,b** and **Figure 2a,b**). They both consist of two domains, with the substrate bound at the interface approximately halfway across the membrane. The transitions between outward- and inward-facing states involve movements of the domains relative to each other. Substrate binding is associated with further local rearrangements of gating elements, which are often formed by discontinuous helices. However, there are clear differences. First, the domains are structurally symmetric in rocker switches but are distinct in rocking bundles. Furthermore, there are obvious differences in gating events. For example, in comparing LeuT and GLUTs it is clear that the extracellular gate of LeuT is larger and more intricate, directly linking several regions to discontinuous helices, Na^+ ions, and substrate (103, 116) (**Figure 3b** and **Figure 4b**). Furthermore, gating rearrangements appear to vary substantially among rocking-bundle transporters with the same fold (103–105, 113, 114, 116). Presumably, these differences reflect the specialization of the structurally distinct bundles in rocking-bundle proteins that may facilitate evolutionary diversification when compared with the structurally similar bundles found in rocker-switch proteins.

It is unclear why rocking-bundle proteins have evolved more elaborate substrate translocation pathways compared with rocker-switch proteins. It is possible that the pathway being selected for is partly driven by a need for more stringent coupling of the substrate with a particular driving solute. In agreement with this line of reasoning, thus far, facilitative, passive transporters have been found to only utilize rocker-switch mechanisms. In bacterial homologs of GLUT transporters, the addition of a single acidic residue to TM1 is sufficient to switch between facilitative and proton-coupled sugar uptake (62). In the multidrug MFS transporter MdfA, an essential proton-coupling acidic residue can be moved to a different helix without disrupting proton-driven transport (128). Also, MdfA transport can be easily switched from being electroneutral to electrogenic by either rational design or random mutagenesis (129). In the oligopeptide- H^+ MFS symporter Pept_{St}, the proton-to-peptide stoichiometry even appears to change depending on the length of the peptide being transported (130). These examples highlight the apparent plasticity of rocker-switch proteins as compared to rocking-bundle transporters, in which there are few, if any, examples that show such a high degree of ion-coupling promiscuity.

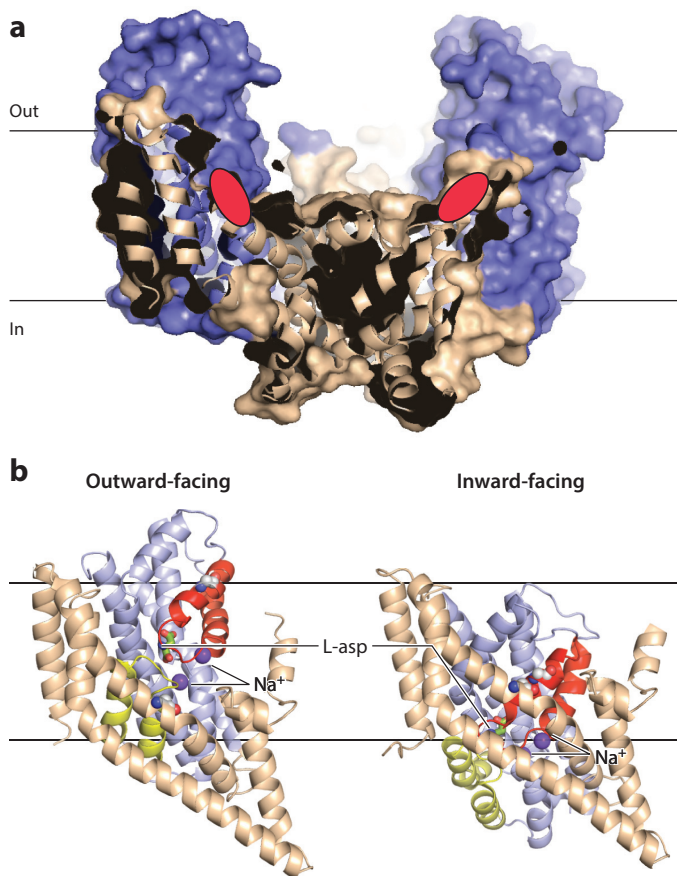


Figure 5

Architecture of the glutamate transporter Glt_{ph}. (a) Bowl-shaped structure formed by the thinner trimeric scaffold (*wheat*) and thicker transport domains (*purple*) [Protein Data Bank (PDB) identification number 2NWL]. Red ellipsoids highlight the location of substrate-binding sites at the bottom of the bowl. Similar concave structures, facing either extracellular or intracellular solutions, have been observed in several other elevator transporters. (b) Schematic representation of Glt_{ph} in the (*left*) outward- and (*right*) inward-facing states (PDB identification numbers 2NWL and 3KBC). The color scheme is as in panel *a* except that the reentrant helical hairpins HP1 and HP2, which constitute substrate gates, are colored *lime green* and *red*, respectively. The substrate and two sodium ions are highlighted as sticks and balls, respectively. Panel *b* is adapted with permission from Reference 18.

THE ELEVATOR MODEL

The Architecture of Elevator Transporters

In the elevator alternating-access mechanism, the substrate-binding site is confined largely, or entirely, to a single domain that traverses the membrane against a relatively rigid, immobile scaffold domain (Figure 1c and Figure 5). Several architecturally distinct proteins whose crystal structures have been determined in recent years appear to function using this mechanism (18–22, 24–26). Similar to rocking-bundle transporters, elevator transporters are made up of two distinct bundles originating from one polypeptide chain. Most of the characterized transporters in this class are either dimers or trimers. One domain, referred to as the scaffold, mediates oligomerization; the

other domain is peripherally located and is typically referred to as the bundle, core, or transport domain. Importantly, the substrate is initially bound predominantly or exclusively within the transport domain. It is translocated across the membrane as the transport domain undergoes a large rigid-body movement against the scaffold (**Figure 1c**). Thus, rather than the two domains moving around the binding site to alternate accessibility to either side of the membrane, the substrate is carried across the membrane by only one of the two domains.

A homolog of glutamate transporters from *Pyrococcus horikoshii*, the sodium–aspartate symporter Glt_{ph} is a founding member of the group of transporters with an elevator transport mechanism (**Figure 2c** and **Figure 5**). Elevator-like movements of the transport domain in Glt_{ph} have been demonstrated crystallographically (18, 132, 133, 164), by EPR (134, 135), and by single-molecule FRET (smFRET) spectroscopy, both in detergent and in liposomes (136–138). Homotrimeric Glt_{ph} is composed of a central trimeric scaffold and three peripheral transport domains. The transport domains undergo a combination of rotational and translational movements that lead to an approximately 18 Å inward translation of the substrate-binding site against the scaffold domain (**Figure 5b**). Remarkably, computationally swapping the conformations of inverted structural repeats in the crystal structure of the outward-facing Glt_{ph} led to the prediction of the elevator-like movements (139); similar repeat-swap models have also been used to predict opposite-facing conformations of both rocker-switch and rocking-bundle proteins (17, 50, 55).

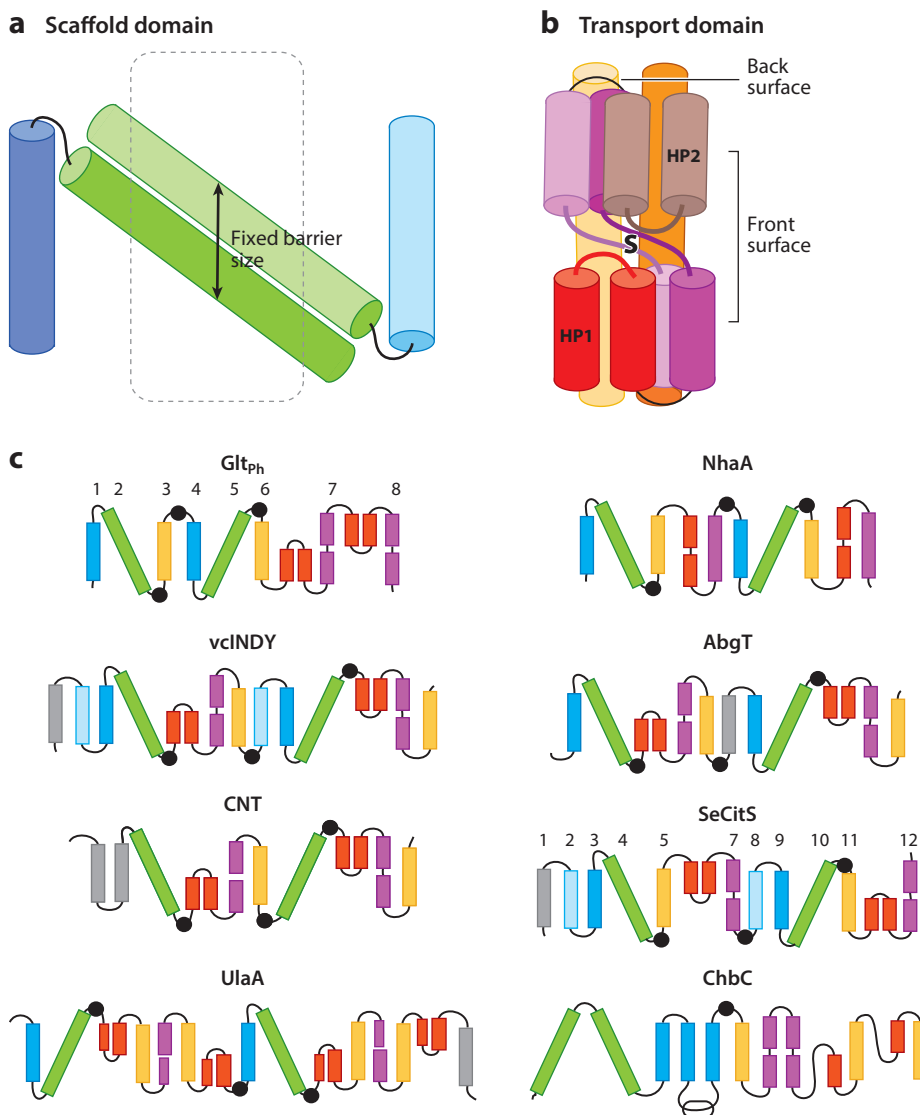
Glt_{ph} is made up of eight TM segments and two reentrant helical hairpins, HP1 and HP2 (**Figure 6**). Unlike most transporters, Glt_{ph} contains two pairs of structurally inverted repeats organized in the following manner—(TM1-3)¹-(TM4-6)² and (HP1-TM7)¹-(HP2-TM8)² (**Figure 6**). The first two TM segments in each of the three-TM-segment repeats form the trimeric scaffold, which is made up of two juxtaposed V-like structural motifs and is reminiscent of the scaffold domain found in LeuT fold transporters (**Figure 6a**). The highly tilted scaffold TM segments 2 and 5 interact with the transport domain in both outward- and inward-facing conformations. The remaining segments—TM3, TM6, and HP1-TM7-HP2-TM8—form the transport domain (**Figure 6b**). The tips of HP1 and HP2, together with the central regions of TM7 and TM8, are key contributors to the substrate-binding site and, in a recurring theme, contain flexible, unwound regions. The two hairpins, together with N-terminal half-helices of TM segments 7 and 8, form the front surface of the transport domain (**Figure 6b**). During the

Figure 6

Topologies of elevator transporters. (a) Frequently observed organization of the scaffold domains, comprising two structurally symmetric, juxtaposed V-like transmembrane (TM) motifs. (b) Organization of the transport domain observed in the glutamate transporter homolog Glt_{ph} and seen with variations in other transporters. Helical hairpin (HP) motifs, together with the TM segments containing either breaks or distortions, make up the front scaffold-facing surface. The back surface is made up of lipid-facing helices. (c) Topologies for representatives of the folds that are either known or expected to work by an elevator mechanism. TM segments related by pseudosymmetry are shown in the same color; helices that do not belong to the inverted structural repeats are gray. Phosphorylation-coupled saccharide transporter ChbC lacks the inverted structural repeats. For this protein, the color scheme was selected to highlight TM segments with a structural equivalence to TM segments in other elevator transporters. Blue and green helices show the characteristic V-shaped motif of the scaffold domains. The blue helices tend to be perpendicular to the membrane, and the green helices are positioned at an oblique angle. Note that the sodium–nucleoside symporter vcCNT lacks the blue helices. Orange, red, and magenta TM segments show the transport domains. Reentrant elements and crossover helices of the Na⁺–H⁺ antiporter NhaA are red. Helices with breaks and distortions that contribute to the binding sites are magenta. Helices facing lipid are orange. β-strands in an ascorbate transporter UlaA are indicated with thinner rectangles. Black circles represent the locations of the loops and helices that connect the scaffold and transport domains.

transport cycle, HP1 and TM7 predominantly face either the scaffold or the intracellular milieu. Conversely, HP2 and TM8 face either the scaffold or the extracellular solution (**Figure 5b**). The pseudosymmetric helices, TM segments 3 and 6, form the backside of the transport domain that always faces lipid. The transport domain is tethered to the scaffold domain by labile loops and helices that facilitate its movements up and down—i.e., like an elevator (18).

The transport domain is compact and cylindrical in shape, with the front side being relatively polar (facing the scaffold) and the backside being hydrophobic (facing the lipid) (**Figure 6b**). The relative polarity of the front side of the transport domain reflects its dual lifestyle, whereby it interacts predominantly either with the scaffold domain or with the bulk solvent (**Figure 1c**). The central part of the scaffold is made of two antiparallel, pseudosymmetric, highly tilted TM segments (**Figure 5b** and **Figure 6a**). These TM segments determine the size of the barrier between the extracellular and intracellular aqueous regions, which is significantly narrower than



the lipid bilayer. Hence, the substrate-binding site within the transport domain does not need to traverse the entire thickness of the membrane. Instead, significantly smaller rearrangements are sufficient to translocate the substrate. The scaffold surface that faces the transport domain is constitutively buried and quite hydrophobic. Thus, the scaffold forms a hydrophobic fixed barrier, and its thickness is determined by how much the helices are tilted relative to the plane of the membrane. The highly tilted two-helix motif is also observed in rotary ATPases, where these helices form the hydrophobic barrier between two half-channels, which ions (either protons or Na^+ ions) traverse during transport (140, 141).

Another two families of transporters that have been proposed to operate by an elevator mechanism are bile acid–sodium symporters and Na^+ – H^+ antiporters, which unexpectedly share the same fold. These conclusions are based on a series of crystal structures of transporters originating from several bacterial species captured in outward- and inward-facing conformations (19, 142–147, 148). Although it seems clear there is an elevator-like movement in bile transporters (143, 144) and in NapA Na^+ – H^+ antiporters (19, 148), the mechanism has also been interpreted as a rocking bundle in MjNhaP1 Na^+ – H^+ antiporters (146). Two-dimensional electron crystallography structures have nonetheless shown that Na^+ – H^+ antiporters are dimers in a lipid environment and that they oligomerize through their scaffold domains (149, 150). Consistently, upon the addition of substrate to two-dimensional crystals, conformational changes have been clearly observed only in the transport domain, and helices in the scaffold domain show little, or no, movement (150).

Transporters with an NhaA fold contain a conserved, structurally inverted repeat of five TM segments, which, as in Glt_{Ph} is similarly organized into scaffold and transport domains (**Figure 6c** and **Figure 7a**). The scaffold domain is formed by the first two TM segments in each five-TM-segment repeat, which display the characteristic V-shaped motif. Interestingly, NapA, PaNhaP, and MjNhaP1 transporters have an additional N-terminal helix that expands the structurally inverted repeat from five to six TM segments (19, 145, 146). This expansion creates a larger oligomerization interface, as scaffold domain interactions are predominantly formed between this additional N-terminal helix and its symmetry partner TM7 on the neighboring protomer. The conserved six-TM-segment transport domain is made up of two three-TM-segment structural repeats that form a compact cylindrical shape similar to Glt_{Ph} . But unlike Glt_{Ph} , transporters with the NhaA fold do not have helical hairpins. They are, however, the only transporter fold known to have two discontinuous pseudosymmetric helices that cross over at their break points (142, 143). Structurally, these crossover helices look like hairpins that have been joined together (**Figure 7a**). Like the hairpins, they constitute critical elements of the substrate-binding sites (142, 143). When the outward-facing structure of NapA was compared with the inward-facing structure of NhaA, it was proposed that the essential ion-binding aspartate in the transport domains shifted inward by approximately 10 Å in the direction normal to membrane plane (19, 142). This elevator movement has recently been confirmed by the structure of the NapA protein captured in an inward-facing conformation (**Figure 7**) (148). However, because monomeric mutants of *E. coli* NhaA are functional (151) and because bacterial bile acid–sodium symporter homologs are monomeric (143, 144), further experimental data are required to put the elevator mechanism for all NhaA-fold members on a firmer footing.

A recent crystal structure of Na^+ –citrate symporter from *Salmonella enterica* SeCitS revealed that these transporters also function by an elevator mechanism. The structure captured SeCitS dimers in an asymmetric state, with one protomer in the outward-facing state and the other in the inward-facing state (24). In SeCitS, the substrate binding site is translocated approximately 16 Å across the membrane as a result of rigid-body movement of the transport domain.

Several apparently evolutionarily unrelated transporter families show structural features consistent with an elevator-like mechanism, although the mechanism has yet to be proved experimentally. These include the sodium–dicarboxylate symporter vcINDY (22, 23), the sodium–nucleoside

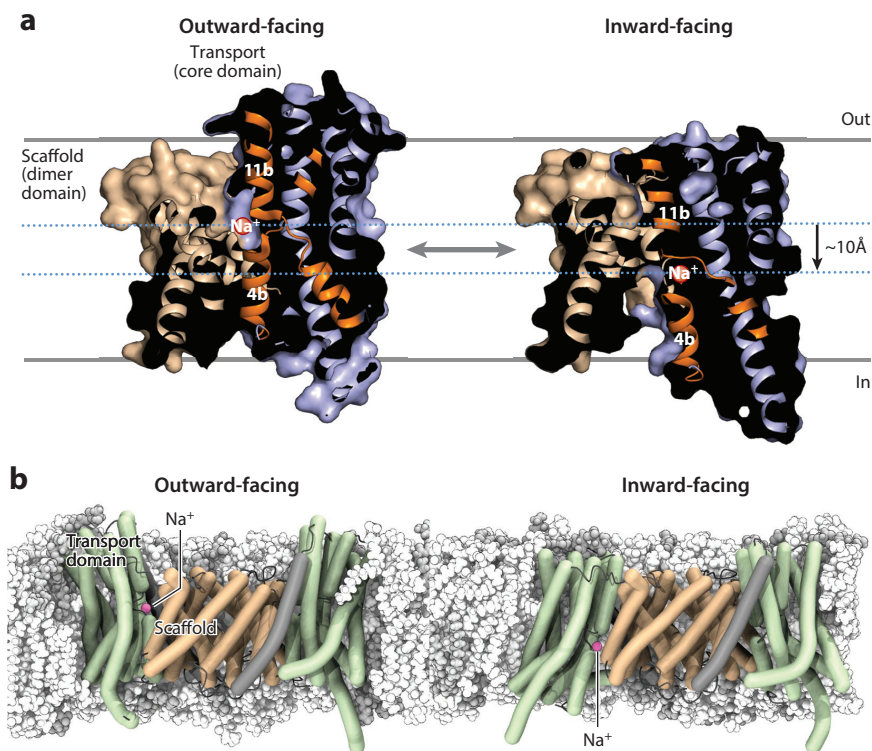


Figure 7

Architecture and elevator mechanism of the sodium–proton antiporter NapA. (a) Schematic representation of Na^+/H^+ antiporter NapA in the (left) outward- and (right) inward-facing states [Protein Data Bank (PDB) identification numbers 5BZZ and 5BZ3]. The scaffold and transport domains are colored wheat and light purple, respectively. The discontinuous helices in the transport domain involved in ion binding and gating are further colored in orange. Transitions between the states involve rigid-body movements of the transport domains along the protein surface provided by the thinner scaffold domain. To alternate accessibility, the ion-binding site is translocated vertically by approximately 10 Å (orange sphere) (148). (b) Schematic representation showing the bowl-shaped NapA structure formed by the thinner dimer scaffold (wheat) and thicker transport domains (green). The outward- and inward-facing structures of the NapA dimer were further embedded into a model membrane bilayer using MD simulations. White lipids are POPE, gray/silver lipids are POPG, and lipids in front were removed for clarity. The position of the ion-binding site (pink) and the ion permeation pathways in a lipid bilayer are shown. Adapted with permission from Reference 19.

symporter vcCNT (25), and p-aminobenzoyl-glutamate AbgT transporters (26, 27). All three families architecturally resemble Glt_{Ph} and SeCitS: They are either dimers (vcINDY and AbgT transporters) or trimers (vcCNT) that consist of a central oligomerization domain and peripheral bundle or transport domains that contain the substrate-binding sites. The three families appear to have different topologies from one another (Figure 6c), although AbgT transporters may share the same fold as vcINDY (152). The scaffold domains of both the AbgT transporters and vcINDY contain two pseudosymmetric V-shaped motifs, similar to those of Glt_{Ph} , SeCitS, and NhaA. However, in vcINDY there is an additional pair of pseudosymmetric N-terminal TM segments that are also part of the scaffold domain. Interestingly, in vcCNT, the V motif is absent, reduced to only a single pair of highly tilted and pseudosymmetric TM segments: Nonsymmetrically related TM segments reinforce the scaffold instead. Overall, the transport domains are similar to those

seen in Glt_{Ph}, featuring pairs of structurally symmetric HPs and discontinuous helices, which make up the central elements of the substrate-binding sites.

Structurally and evolutionarily unrelated phosphorylation-coupled ascorbate and saccharide transporters are parts of phosphotransferase systems (20, 21). They mediate the passive influx of their substrates into cells in a process coupled to substrate phosphorylation in the cytoplasm. Both families are thought to function by elevator-like mechanisms. UlaA, an ascorbate transporter from *E. coli*, is a dimer that has been captured crystallographically in two conformations: one in which its transport domain is in the outward position and the other in which it has partially moved inward (21). It contains two inverted structural repeats that contribute to the scaffold and transport domains. Its scaffold is quite similar to those described for the abovementioned elevator transporters. In contrast, the transport domain appears to be architecturally distinct, although it does contain reentrant elements that coordinate substrates. However, these are not helix-turn-helix hairpin motifs, but rather β -strand-turn-helix motifs. Moreover, there are two of them per pseudosymmetric repeat (**Figure 6c**).

The phosphotransferase system saccharide transporter does not seem to adhere to most of the structural principles outlined here (20). In particular, the crystal structure of an *E. coli* homolog, ChbC, revealed an unexpected absence of any structurally inverted repeats (20). Nevertheless, similar to other transporters, ChbC still partitions into two domains: a scaffold and a substrate-containing transport domain. ChbC is dimeric, and the dimer interface is primarily composed of two tilted TM segments, 1 and 2, which are reminiscent of the tilted TM segments in other transporters. TM segments 3, 4, and 5 also contribute to the scaffold domain (**Figure 6c**). The remainder of the protein forms the transport domain, which contains two reentrant hairpins (HP1 and HP2) and a discontinuous and a distorted helix (TM segments 7 and 8). In an interesting deviation from other elevator proteins, both subunits of the dimer contribute to the substrate-binding sites in the inward-facing state such that the soluble loop in the scaffold domain of one protomer serves as a lid for the substrate-binding site in another protomer.

Extreme Asymmetry of Domains in Elevator-Like Transporters

The clear functional specialization of the two domains in the elevator transporters is obvious from their structural variations from one another. Interestingly, all scaffold domains known thus far seem to share a similar motif of two highly tilted, antiparallel TM helices (**Figure 6a**). These TM segments form the key barrier between the aqueous milieus on the opposite sides of the membrane. Another defining feature is that the scaffold domain is much shorter than the transport domain; indeed, some scaffold helices approximately normal to the lipid bilayer are only 14 amino acids long (19). This significant difference in dimensions is not observed in either rocker-switch or rocking-bundle transporters, where both domains are of comparable thickness (**Figure 2**). Because of this difference in size, oligomeric elevator proteins form water-filled bowls in the membrane in at least one of their alternate conformational states (**Figure 5a** and **Figure 7b**). Therefore, a scaffold domain facilitates substrate access to its binding site by simply being shorter, and as such, the substrate does not need to first traverse through a deep protein cavity. Indeed, the substrate-binding sites are typically located at the bottom of the bowl (**Figure 5a** and **Figure 7b**). The membrane likely adapts to the thinner hydrophobic scaffold domain due to hydrophobic mismatch, and the proteinaceous bowl likely allows water to enter. Collectively, these factors facilitate substrate diffusion to the binding site. The defining feature of elevator proteins is that most, if not all, residues essential for substrate recognition and binding are contained within the transport domain. In the Na⁺-H⁺ antiporters NapA and MjNhaP1, the outer surface of the

scaffold domain is negatively charged, which presumably helps to select for, and concentrate, its substrate as it traverses from the surface down into the substrate-binding site (19, 146) (**Figure 7b**).

Substrate Binding and Gating

Because the substrate is transported within only one of the domains, we expect gating to also be confined to that one domain. Unfortunately, for a majority of elevator proteins, with the exception of the outward-facing state of Glt_{ph} and, partially, the inward-facing SeCitS, gating events have not yet been structurally resolved (24, 154). Reentrant loops, often in the form of helical hairpins, are found in most elevator transport domains, and they contribute principally to substrate-binding sites in vcINDY, vcCNT, ChbC, UlaA, SeCitS, and Glt_{ph} (20–22, 24, 25, 132). They are also well suited for restricting the conformational changes associated with gating to the transport domain. This is clearly illustrated in Glt_{ph}. In the outward-facing state of Glt_{ph}, HP2, which is known to serve as the substrate gate (132, 153–156), has no interactions with the scaffold domain (**Figure 5b**). Thus, HP2 is free to open and close without accompanying structural changes in the scaffold. Notably, restricting gating events to a single domain might not be possible in ChbC, in which the scaffold loop of the neighboring subunit contributes to the binding site (20). In Glt_{ph}, the substrate aspartate is completely occluded under the tips of HP1 and HP2 in both outward- and inward-facing states (18, 132, 133). In other transporters, the occlusion is incomplete but significant (21, 22, 24, 25). Though the gating movements by HPs appear to be less extensive, they likely constitute at least part of the gating mechanism. In Na⁺–H⁺ antiporters, the substrate binds outside of the discontinuous helix crossover (19, 142, 145, 146). Almost certainly, only small gating movements are required to bind and release ions in this fold. Complete occlusion in elevator transporters must, however, take place during movement of the transport domain, when the substrate becomes buried at the interface between the transport domain and the scaffold.

The mechanism of coupling local gating motions and global structural transitions appears to be different in elevators, rocking-switch transporters, and rocking-bundle transporters. As we have discussed for GLUTs, local closure of the extracellular gates might be linked to the global conformational transition through mechanical coupling, whereby the gate closure distorts an interacting helix, a strain that is relieved through the disruption of the intracellular, interbundle interactions that permit the rocking switch to operate (78) (**Figure 3b**). In elevator transporters, the coupling might be achieved because the translocation of the transport domains is sterically hindered as long as the gates remain open. Once the gates assume a translocation-competent conformation, the domain movement might simply be a stochastic process driven by thermal energy. Glt_{ph} and a closely related transporter, Glt_{Tk}, were crystallized in the absence of substrate and ions (154, 157). Interestingly, an occluded state is still formed, showing closed hairpins similar to the fully bound transporters, albeit somewhat structurally rearranged. It is unknown whether this propensity to easily form the fully occluded state in the absence of substrates is specific to Glt_{ph} and related proteins or is typical of other elevator-like transporters. During transport, elevator proteins seem to demonstrate a remarkable structural integrity in the transport domain fold, which remains essentially unaltered during rigid-body rearrangements from the outward- to inward-facing conformations (18, 24, 148).

Glt_{ph}, vcINDY, vcCNT, SeCitS, and bile-acid transporters are all driven by sodium electrochemical gradients (23–25, 132, 158, 158a). Thus, all of these transporters have to achieve coupled transport and prevent uncoupled ion leak. Based on current knowledge, the mechanisms that elevator-like transporters use to achieve such coupling do not fundamentally differ from rocker-switch and rocking-bundle transporters. These include cooperative binding between Na⁺ ions and substrate, and the requirement that both solutes are bound before the local protein gates

are fully closed and the translocation step is permitted. In Glt_{ph}, both of these mechanisms are at play (154, 159). First, sodium and aspartate bind with high cooperativity. Structural comparisons of substrate-free, sodium-bound, and sodium–aspartate-bound transporters suggest that sodium binding induces a conformational change in the transporter that primes it for substrate binding. The energetic penalty that the ions pay in the process is the origin of cooperativity: Once sodium ions bind, aspartate binds to an already preformed site. The cooperative binding of substrate and ions explains why substrate alone cannot be transported (it simply does not bind with appreciable affinity). Crystallization of the mutant Glt_{ph} transporter with low intrinsic substrate affinity loaded only with Na⁺ ions and no substrate showed an outward-facing conformation with an open HP2 gate (154). Thus, to prevent the transport of sodium ions alone, the transporter uses an additional mechanism, whereby the extracellular gate remains open in the sodium-only bound state. Not all transporters show sodium-dependent structural changes as Glt_{ph} does. For example, the bacterial bile acid–sodium symporter homologs have essentially identical structures when only one of the two sodium sites is occupied (144).

CONCLUSIONS AND FUTURE PERSPECTIVES

The Dynamics of Structural Transitions

It seems that in many transporters, regardless of the alternating-access mechanism, the outward- and inward-facing states are nearly equienergetic under isotropic solution conditions (i.e., in detergent solutions or in the presence of symmetric *trans*-membrane solute concentrations). It has consistently been demonstrated that several transporters can be crystallized in several states under identical, or nearly identical, conditions. For some transporters, including LacY, LeuT, and Glt_{ph}, the state distributions have been measured directly using EPR, smFRET, or both (88, 134–138, 160, 161). These experiments have demonstrated that the probed transporters sampled both outward- and inward-facing states, regardless of whether they were bound to their substrates or empty. The binding of ions and substrate thermodynamically favors either outward- or inward-facing states (whichever one has the higher affinity for the solutes). Under nonequilibrium physiologic conditions—e.g., in the presence of comparatively high sodium concentrations in the extracellular solution—ion binding from outside would, of course, favor the outward-facing state of sodium-coupled transporters.

Although the state distribution of transporters may not be significantly affected by substrate binding under isotropic conditions, it is generally believed that substrate facilitates global transitions between the states. This notion is supported by numerous functional studies of transporters and by spectroscopic experiments, such as smFRET studies conducted on LeuT and LacY (88, 161). As we have described above, in these transporters substrate binding on the interface of the rocking domains likely facilitates the process by favoring gate closure and, perhaps, other mechanisms. In elevator transporters, this might not necessarily be the case. In Glt_{ph}, for example, HP2 appears to spontaneously close in the substrate-free state and, therefore, substrate may not serve as a catalyst of the transition. Studies using smFRET, in which the movements of the transport domain have been observed directly, consistently seem to suggest that the translocation of the substrate-loaded transport domain is the slowest step of the transport cycle (137, 138). This feature may well be peculiar to Glt_{ph}, which is a homolog from a hyperthermophilic archaeon. Indeed, in the mammalian transporters, the return of the substrate-free (K⁺-bound) transport domain into the outward position has been shown to be rate limiting (162). More studies of transporter dynamics are required before general rules can be established.

Interestingly, recent observations in NapA, Glt_{ph}, and SeCitS crystal structures suggest that hydrocarbon chains of lipids and detergents may enter the interface between the transporter domains, perhaps facilitating their relative movements (24, 138, 148). Further studies are needed to clarify the effect of interface solvation by water and lipids on protein function and dynamics.

Summary

The functional units of transporters tend to comprise two domains that move relative to each other to provide alternating access to the substrate-binding site; mitochondrial exchangers may represent one of just a few exceptions (163). In the evolutionary progression of diminishing structural symmetry between the domains, from the highly symmetric SWEETs and EmrE through to more complex, less symmetric rocker-switch and rocking-bundle transporters, elevator transporters constitute an extreme form of asymmetry (**Figure 2**). This asymmetry occurs parallel to increased functional specialization, in which both binding and transport are carried out in just one of the two domains. In the rocker-switch and rocking-bundle transporters, it is not always obvious which of the two domains does the rocking and which remains stationary in the membrane, and in simple rocker-switch transporters both domains might be moving, such as in the SWEETs and EmrE. Furthermore, in proteins sharing the same fold (such as the LeuT fold), distinct domains have been implicated as being labile. This ambiguity is of course possible only in monomeric proteins in which there are no physical constraints to limit the movement of one of the domains—for example, monomeric MFS and LeuT fold transporters or dimeric SWEETs and EmrE. The majority of the elevator transporters, however, are oligomers associating through extensive interactions between scaffold domains. In such oligomers, only the transport domains are free to move extensively. The only way in which this constraint could be broken is in a hypothetical situation, in which all scaffold domains move together, requiring strict cooperativity among subunits. However, to the best of our knowledge, intersubunit cooperativity is not common in elevator transporters.

It seems likely that the three mechanisms outlined here describe the bulk of secondary active transport, but knowledge of topological and structural diversity will continue to grow. Where we believe significant knowledge gaps exist is in the understanding of how these multiple transporter states relate to one another energetically and dynamically, what the transition pathways are between them, and what constitutes the critical energetic barriers. Although crystallography may provide some insights, and intermediate states have been pictured in several transporters, including, for example, BetP (113), Glt_{ph} (164), and UlaA (21), major progress will likely come from combining structural studies with investigations of protein dynamics using smFRET, nuclear magnetic resonance, and other approaches that are sensitive to molecular dynamics. Lastly, the activities of many transporters, particularly those of mammalian origin, are exquisitely regulated by extrinsic factors. Realistically, the molecular basis of their allosteric regulation and dynamics can be understood only by obtaining high-resolution structures of these proteins in complex with their allosteric modulators, and then combining this information with advanced biochemical, biophysical, and computational approaches. Clearly, there are many important and challenging questions that need to be addressed.

DISCLOSURE STATEMENT

The authors are not aware of any affiliations, memberships, funding, or financial holdings that might be perceived as affecting the objectivity of this review.

ACKNOWLEDGMENTS

We thank Alex Cameron and Oliver Beckstein for assistance in generating **Figures 4a** and **7b**. We gratefully acknowledge support from the Knut and Alice Wallenberg Foundation (D.D.), the Swedish Research Council (D.D.), the EMBO Young Investigator Program (D.D.), the National Institutes of Health (O.B.), and the Howard Hughes Medical Institute Investigator Program (O.B.).

LITERATURE CITED

1. Mitchell P. 1957. A general theory of membrane transport from studies of bacteria. *Nature* 180:134–36
- 1a. Mitchell P. 1990. Osmochemistry of solute translocation. *Res. Microbiol.* 141:286–89
2. Patlak CS. 1957. Contributions to the theory of active transport: II. The gate type non-carrier mechanism and generalizations concerning tracer flow, efficiency, and measurement of energy expenditure. *Bull. Math. Biophys.* 19:209–35
3. Jardetzky O. 1966. Simple allosteric model for membrane pumps. *Nature* 211:969–70
4. Abramson J, Smirnova I, Kasho V, Verner G, Kaback HR, Iwata S. 2003. Structure and mechanism of the lactose permease of *Escherichia coli*. *Science* 301:610–15
5. Ethayathulla AS, Yousef MS, Amin A, Leblanc G, Kaback HR, Guan L. 2014. Structure-based mechanism for Na⁺/melibiose symport by MelB. *Nat. Commun.* 5:3009
6. Accardi A, Miller C. 2004. Secondary active transport mediated by a prokaryotic homologue of ClC Cl⁻ channels. *Nature* 427:803–7
7. Dutzler R, Campbell EB, Cadene M, Chait BT, MacKinnon R. 2002. X-ray structure of a ClC chloride channel at 3.0 Å reveals the molecular basis of anion selectivity. *Nature* 415:287–94
8. Dutzler R, Campbell EB, MacKinnon R. 2003. Gating the selectivity filter in ClC chloride channels. *Science* 300:108–12
9. Feng L, Campbell EB, Hsiung Y, MacKinnon R. 2010. Structure of a eukaryotic CLC transporter defines an intermediate state in the transport cycle. *Science* 330:635–41
10. Elvington SM, Liu CW, Maduke MC. 2009. Substrate-driven conformational changes in ClC-ec1 observed by fluorine NMR. *EMBO J.* 28:3090–102
11. Basilio D, Noack K, Picollo A, Accardi A. 2014. Conformational changes required for H⁺/Cl⁻ exchange mediated by a CLC transporter. *Nat. Struct. Mol. Biol.* 21:456–63
12. Abraham SJ, Cheng RC, Chew TA, Khantwal CM, Liu CW, et al. 2015. ¹³C NMR detects conformational change in the 100-kD membrane transporter ClC-ec1. *J. Biomol. NMR* 61:209–26
13. Jayaram H, Accardi A, Wu F, Williams C, Miller C. 2008. Ion permeation through a Cl⁻-selective channel designed from a CLC Cl⁻/H⁺ exchanger. *PNAS* 105:11194–99
14. Walden M, Accardi A, Wu F, Xu C, Williams C, Miller C. 2007. Uncoupling and turnover in a Cl⁻/H⁺ exchange transporter. *J. Gen. Physiol.* 129:317–29
15. Accardi A, Picollo A. 2010. CLC channels and transporters: proteins with borderline personalities. *Biochim. Biophys. Acta* 1798:1457–64
16. Yan N. 2015. Structural biology of the major facilitator superfamily transporters. *Annu. Rev. Biophys.* 44:257–83
17. Forrest LR, Rudnick G. 2009. The rocking bundle: a mechanism for ion-coupled solute flux by symmetrical transporters. *Physiology* 24:377–86
18. Reyes N, Ginter C, Boudker O. 2009. Transport mechanism of a bacterial homologue of glutamate transporters. *Nature* 462:880–85
19. Lee C, Kang HJ, von Ballmoos C, Newstead S, Uzdavinyas P, et al. 2013. A two-domain elevator mechanism for sodium/proton antiport. *Nature* 501:573–77
20. Cao Y, Jin X, Levin EJ, Huang H, Zong Y, et al. 2011. Crystal structure of a phosphorylation-coupled saccharide transporter. *Nature* 473:50–54
21. Luo P, Yu X, Wang W, Fan S, Li X, Wang J. 2015. Crystal structure of a phosphorylation-coupled vitamin C transporter. *Nat. Struct. Mol. Biol.* 22:238–41

22. Mancusso R, Gregorio GG, Liu Q, Wang D-N. 2012. Structure and mechanism of a bacterial sodium-dependent dicarboxylate transporter. *Nature* 491:622–26
23. Mulligan C, Fitzgerald GA, Wang DN, Mindell JA. 2014. Functional characterization of a Na⁺-dependent dicarboxylate transporter from *Vibrio cholerae*. *J. Gen. Physiol.* 143:745–59
24. Wöhlert D, Grötzinger MJ, Kühlbrandt W, Yildiz Ö. 2015. Mechanism of Na⁺-dependent citrate transport from the structure of an asymmetrical CitS dimer. *eLife* 4:e09375
25. Johnson ZL, Cheong C-G, Lee S-Y. 2012. Crystal structure of a concentrative nucleoside transporter from *Vibrio cholerae* at 2.4 Å. *Nature* 483:489–93
26. Bolla JR, Su C-C, Delmar JA, Radhakrishnan A, Kumar N, et al. 2015. Crystal structure of the *Alcanivorax borkumensis* YdaH transporter reveals an unusual topology. *Nat. Commun.* 6:6874
27. Su C-C, Bolla JR, Kumar N, Radhakrishnan A, Long F, et al. 2015. Structure and function of *Neisseria gonorrhoeae* MtrF illuminates a class of antimetabolite efflux pumps. *Cell Rep.* 11:61–70
28. ter Beek J, Guskov A, Slotboom DJ. 2014. Structural diversity of ABC transporters. *J. Gen. Physiol.* 143:419–35
29. Yan N. 2013. Structural advances for the major facilitator superfamily (MFS) transporters. *Trends Biochem. Sci.* 38:151–59
30. Karpowich NK, Wang DN. 2008. Structural biology: symmetric transporters for asymmetric transport. *Science* 321:781–82
31. Serdiuk T, Madej MG, Sugihara J, Kawamura S, Mari SA, et al. 2014. Substrate-induced changes in the structural properties of LacY. *PNAS* 111:E1571–80
32. Chen LQ, Hou BH, Lalonde S, Takanaga H, Hartung ML, et al. 2010. Sugar transporters for intercellular exchange and nutrition of pathogens. *Nature* 468:527–32
33. Xuan YH, Hu YB, Chen LQ, Sosso D, Ducat DC, et al. 2013. Functional role of oligomerization for bacterial and plant SWEET sugar transporter family. *PNAS* 110:E3685–94
34. Xu Y, Tao Y, Cheung LS, Fan C, Chen LQ, et al. 2014. Structures of bacterial homologues of SWEET transporters in two distinct conformations. *Nature* 515:448–52
35. Lee Y, Nishizawa T, Yamashita K, Ishitani R, Nureki O. 2015. Structural basis for the facilitative diffusion mechanism by SemiSWEET transporter. *Nat. Commun.* 6:6112
36. Wang J, Yan C, Li Y, Hirata K, Yamamoto M, et al. 2014. Crystal structure of a bacterial homologue of SWEET transporters. *Cell Res.* 24:1486–89
37. von Heijne G. 1992. Membrane protein structure prediction: hydrophobicity analysis and the positive-inside rule. *J. Mol. Biol.* 225:487–94
38. Zhai Y, Heijne WH, Smith DW, Saier MH Jr. 2001. Homologues of archaeal rhodopsins in plants, animals and fungi: structural and functional predications for a putative fungal chaperone protein. *Biochim. Biophys. Acta* 1511:206–23
39. Yee DC, Shlykov MA, Vastermark A, Reddy VS, Arora S, et al. 2013. The transporter-opsin-G protein-coupled receptor (TOG) superfamily. *FEBS J.* 280:5780–800
40. Rotem D, Schuldiner S. 2004. EmrE, a multidrug transporter from *Escherichia coli*, transports monovalent and divalent substrates with the same stoichiometry. *J. Biol. Chem.* 279:48787–93
41. Rapp M, Seppala S, Granseth E, von Heijne G. 2007. Emulating membrane protein evolution by rational design. *Science* 315:1282–84
42. Nara T, Kouyama T, Kurata Y, Kikukawa T, Miyauchi S, Kamo N. 2007. Anti-parallel membrane topology of a homo-dimeric multidrug transporter, EmrE. *J. Biochem.* 142:621–25
43. Nasie I, Steiner-Mordoch S, Gold A, Schuldiner S. 2010. Topologically random insertion of EmrE supports a pathway for evolution of inverted repeats in ion-coupled transporters. *J. Biol. Chem.* 285:15234–44
44. Morrison EA, DeKoster GT, Dutta S, Vafabakhsh R, Clarkson MW, et al. 2012. Antiparallel EmrE exports drugs by exchanging between asymmetric structures. *Nature* 481:45–50
45. Lloris-Garcera P, Bianchi F, Slusky JS, Seppala S, Daley DO, von Heijne G. 2012. Antiparallel dimers of the small multidrug resistance protein EmrE are more stable than parallel dimers. *J. Biol. Chem.* 287:26052–59
46. Korkhov VM, Tate CG. 2008. Electron crystallography reveals plasticity within the drug binding site of the small multidrug transporter EmrE. *J. Mol. Biol.* 377:1094–103

47. Chen YJ, Pornillos O, Lieu S, Ma C, Chen AP, Chang G. 2007. X-ray structure of EmrE supports dual topology model. *PNAS* 104:18999–9004
48. Yerushalmi H, Lebendiker M, Schuldiner S. 1995. EmrE, an *Escherichia coli* 12-kDa multidrug transporter, exchanges toxic cations and H⁺ and is soluble in organic solvents. *J. Biol. Chem.* 270:6856–63
49. Jaehme M, Guskov A, Slotboom DJ. 2014. Crystal structure of the vitamin B3 transporter PnuC, a full-length SWEET homolog. *Nat. Struct. Mol. Biol.* 21:1013–15
50. Forrest LR. 2015. Structural symmetry in membrane proteins. *Annu. Rev. Biophys.* 44:311–37
51. Pao SS, Paulsen IT, Saier MH Jr. 1998. Major facilitator superfamily. *Microbiol. Mol. Biol. Rev.* 62:1–34
52. Lemieux MJ, Huang Y, Wang da N. 2005. Crystal structure and mechanism of GlpT, the glycerol-3-phosphate transporter from *E. coli*. *J. Electron Microsc.* 54(Suppl. 1):i43–46
53. Sun L, Zeng X, Yan C, Sun X, Gong X, et al. 2012. Crystal structure of a bacterial homologue of glucose transporters GLUT1–4. *Nature* 490:361–66
54. Deng D, Xu C, Sun P, Wu J, Yan C, et al. 2014. Crystal structure of the human glucose transporter GLUT1. *Nature* 510:121–25
55. Radestock S, Forrest LR. 2011. The alternating-access mechanism of MFS transporters arises from inverted-topology repeats. *J. Mol. Biol.* 407:698–715
56. Deleted in proof
57. Huang Y, Lemieux MJ, Song J, Auer M, Wang DN. 2003. Structure and mechanism of the glycerol-3-phosphate transporter from *Escherichia coli*. *Science* 301:616–20
58. Dang S, Sun L, Huang Y, Lu F, Liu Y, et al. 2010. Structure of a fucose transporter in an outward-open conformation. *Nature* 467:734–38
59. Quistgaard EM, Low C, Moberg P, Tresaugues L, Nordlund P. 2013. Structural basis for substrate transport in the GLUT-homology family of monosaccharide transporters. *Nat. Struct. Mol. Biol.* 20:766–68
60. Deng D, Sun P, Yan C, Ke M, Jiang X, et al. 2015. Molecular basis of ligand recognition and transport by glucose transporters. *Nature* 526:391–96
61. Wisedchaisri G, Park MS, Iadanza MG, Zheng H, Gonen T. 2014. Proton-coupled sugar transport in the prototypical major facilitator superfamily protein XylE. *Nat. Commun.* 5:4521
62. Iancu CV, Zamoan J, Woo SB, Aleshin A, Choe JY. 2013. Crystal structure of a glucose/H⁺ symporter and its mechanism of action. *PNAS* 110:17862–67
63. Newstead S, Drew D, Cameron AD, Postis VL, Xia X, et al. 2011. Crystal structure of a prokaryotic homologue of the mammalian oligopeptide-proton symporters, PepT1 and PepT2. *EMBO J.* 30:417–26
64. Solcan N, Kwok J, Fowler PW, Cameron AD, Drew D, et al. 2012. Alternating access mechanism in the POT family of oligopeptide transporters. *EMBO J.* 31:3411–21
65. Guettou F, Quistgaard EM, Raba M, Moberg P, Low C, Nordlund P. 2014. Selectivity mechanism of a bacterial homolog of the human drug-peptide transporters PepT1 and PepT2. *Nat. Struct. Mol. Biol.* 21:728–31
66. Doki S, Kato HE, Solcan N, Iwaki M, Koyama M, et al. 2013. Structural basis for dynamic mechanism of proton-coupled symport by the peptide transporter POT. *PNAS* 110:11343–48
67. Zhao Y, Mao G, Liu M, Zhang L, Wang X, Zhang XC. 2014. Crystal structure of the *E. coli* peptide transporter YbgH. *Structure* 22:1152–60
68. Yan H, Huang W, Yan C, Gong X, Jiang S, et al. 2013. Structure and mechanism of a nitrate transporter. *Cell Rep.* 3:716–23
69. Zheng H, Wisedchaisri G, Gonen T. 2013. Crystal structure of a nitrate/nitrite exchanger. *Nature* 497:647–51
70. Sun J, Bankston JR, Payandeh J, Hinds TR, Zagotta WN, Zheng N. 2014. Crystal structure of the plant dual-affinity nitrate transporter NRT1.1. *Nature* 507:73–77
71. Parker JL, Newstead S. 2014. Molecular basis of nitrate uptake by the plant nitrate transporter NRT1.1. *Nature* 507:68–72
72. Fukuda M, Takeda H, Kato HE, Doki S, Ito K, et al. 2015. Structural basis for dynamic mechanism of nitrate/nitrite antiport by NarK. *Nat. Commun.* 6:7097
73. Pedersen BP, Kumar H, Waight AB, Risenmay AJ, Roe-Zurz Z, et al. 2013. Crystal structure of a eukaryotic phosphate transporter. *Nature* 496:533–36

74. Yin Y, He X, Szewczyk P, Nguyen T, Chang G. 2006. Structure of the multidrug transporter EmrD from *Escherichia coli*. *Science* 312:741–44
75. Jiang D, Zhao Y, Wang X, Fan J, Heng J, et al. 2013. Structure of the YajR transporter suggests a transport mechanism based on the conserved motif A. *PNAS* 110:14664–69
76. Hirai T, Subramaniam S. 2004. Structure and transport mechanism of the bacterial oxalate transporter OxlT. *Biophys. J.* 87:3600–7
77. Lyons JA, Parker JL, Solcan N, Brinth A, Li D, et al. 2014. Structural basis for polyspecificity in the POT family of proton-coupled oligopeptide transporters. *EMBO Rep.* 15:886–93
78. Nomura N, Verdon G, Kang HJ, Shimamura T, Nomura Y, et al. 2015. Structure and mechanism of the mammalian fructose transporter GLUT5. *Nature* 526:397–401
79. Seatter MJ, De la Rue SA, Porter LM, Gould GW. 1998. QLS motif in transmembrane helix VII of the glucose transporter family interacts with the C-1 position of D-glucose and is involved in substrate selection at the exofacial binding site. *Biochemistry* 37:1322–26
80. Hruz PW, Mueckler MM. 1999. Cysteine-scanning mutagenesis of transmembrane segment 7 of the GLUT1 glucose transporter. *J. Biol. Chem.* 274:36176–80
81. Mueckler M, Makepeace C. 2002. Analysis of transmembrane segment 10 of the Glut1 glucose transporter by cysteine-scanning mutagenesis and substituted cysteine accessibility. *J. Biol. Chem.* 277:3498–503
82. Kumar H, Kasho V, Smirnova I, Finer-Moore JS, Kaback HR, Stroud RM. 2014. Structure of sugar-bound LacY. *PNAS* 111:1784–88
83. Kumar H, Finer-Moore JS, Kaback HR, Stroud RM. 2015. Structure of LacY with an α -substituted galactoside: connecting the binding site to the protonation site. *PNAS* 112:9004–9
84. Stelzl LS, Fowler PW, Sansom MS, Beckstein O. 2014. Flexible gates generate occluded intermediates in the transport cycle of LacY. *J. Mol. Biol.* 426:735–51
85. Fowler PW, Orwick-Rydmark M, Radestock S, Solcan N, Dijkman PM, et al. 2015. Gating topology of the proton-coupled oligopeptide symporters. *Structure* 23:290–301
86. Lowe AG. 1989. The kinetics and thermodynamics of glucose transport in human erythrocytes: indications for the molecular mechanism of transport. *Biochem. Soc. Trans.* 17:435–38
87. Mueckler M, Thorens B. 2013. The SLC2 (GLUT) family of membrane transporters. *Mol. Asp. Med.* 34:121–38
88. Majumdar DS, Smirnova I, Kasho V, Nir E, Kong X, et al. 2007. Single-molecule FRET reveals sugar-induced conformational dynamics in LacY. *PNAS* 104:12640–45
89. Kaback HR. 2015. A chemiosmotic mechanism of symport. *PNAS* 112:1259–64
90. Klingenberg M. 2005. Ligand–protein interaction in biomembrane carriers: the induced transition fit of transport catalysis. *Biochemistry* 44:8563–70
91. Law CJ, Almqvist J, Bernstein A, Goetz RM, Huang Y, et al. 2008. Salt-bridge dynamics control substrate-induced conformational change in the membrane transporter GlpT. *J. Mol. Biol.* 378:828–39
92. Mirza O, Guan L, Verner G, Iwata S, Kaback HR. 2006. Structural evidence for induced fit and a mechanism for sugar/H⁺ symport in LacY. *EMBO J.* 25:1177–83
93. Smirnova IN, Kasho V, Kaback HR. 2008. Protonation and sugar binding to LacY. *PNAS* 105:8896–901
94. Andersson M, Bondar AN, Freitas JA, Tobias DJ, Kaback HR, White SH. 2012. Proton-coupled dynamics in lactose permease. *Structure* 20:1893–904
95. Manolescu A, Salas-Burgos AM, Fischbarg J, Cheeseman CI. 2005. Identification of a hydrophobic residue as a key determinant of fructose transport by the facilitative hexose transporter SLC2A7 (GLUT7). *J. Biol. Chem.* 280:42978–83
96. Kasahara T, Maeda M, Boles E, Kasahara M. 2009. Identification of a key residue determining substrate affinity in the human glucose transporter GLUT1. *Biochim. Biophys. Acta* 1788:1051–55
97. Maiden MC, Davis EO, Baldwin SA, Moore DC, Henderson PJ. 1987. Mammalian and bacterial sugar transport proteins are homologous. *Nature* 325:641–43
98. Schurmann A, Doege H, Ohnimus H, Monser V, Buchs A, Joost HG. 1997. Role of conserved arginine and glutamate residues on the cytosolic surface of glucose transporters for transporter function. *Biochemistry* 36:12897–902

99. Tanaka Y, Hipolito CJ, Maturana AD, Ito K, Kuroda T, et al. 2013. Structural basis for the drug extrusion mechanism by a MATE multidrug transporter. *Nature* 496:247–51
100. Lu M, Radchenko M, Symersky J, Nie R, Guo Y. 2013. Structural insights into H⁺-coupled multidrug extrusion by a MATE transporter. *Nat. Struct. Mol. Biol.* 20:1310–17
101. Lu M, Symersky J, Radchenko M, Koide A, Guo Y, et al. 2013. Structures of a Na⁺-coupled, substrate-bound MATE multidrug transporter. *PNAS* 110:2099–104
102. Radchenko M, Symersky J, Nie R, Lu M. 2015. Structural basis for the blockade of MATE multidrug efflux pumps. *Nat. Commun.* 6:7995
103. Yamashita A, Singh SK, Kawate T, Jin Y, Gouaux E. 2005. Crystal structure of a bacterial homologue of Na⁺/Cl⁻-dependent neurotransmitter transporters. *Nature* 437:215–23
104. Weyand S, Shimamura T, Yajima S, Suzuki S, Mirza O, et al. 2008. Structure and molecular mechanism of a nucleobase-cation-symport-1 family transporter. *Science* 322:709–13
105. Ressler S, Terwisscha van Scheltinga AC, Vonrhein C, Ott V, Ziegler C. 2009. Molecular basis of transport and regulation in the Na⁺/betaine symporter BetP. *Nature* 458:47–52
106. Faham S, Watanabe A, Besserer GM, Cascio D, Specht A, et al. 2008. The crystal structure of a sodium galactose transporter reveals mechanistic insights into Na⁺/sugar symport. *Science* 321:810–14
107. Gao X, Lu F, Zhou L, Dang S, Sun L, et al. 2009. Structure and mechanism of an amino acid antiporter. *Science* 324:1565–68
108. Shaffer PL, Goehring A, Shankaranarayanan A, Gouaux E. 2009. Structure and mechanism of a Na⁺-independent amino acid transporter. *Science* 325:1010–14
109. Tang L, Bai L, Wang WH, Jiang T. 2010. Crystal structure of the carnitine transporter and insights into the antiport mechanism. *Nat. Struct. Mol. Biol.* 17:492–96
110. Penmatsa A, Gouaux E. 2014. How LeuT shapes our understanding of the mechanisms of sodium-coupled neurotransmitter transporters. *J. Physiol.* 592:863–69
111. Shi Y. 2013. Common folds and transport mechanisms of secondary active transporters. *Annu. Rev. Biophys.* 42:51–72
112. Claxton DP, Quick M, Shi L, de Carvalho FD, Weinstein H, et al. 2010. Ion/substrate-dependent conformational dynamics of a bacterial homolog of neurotransmitter:sodium symporters. *Nat. Struct. Mol. Biol.* 17:822–29
113. Perez C, Koshy C, Yildiz O, Ziegler C. 2012. Alternating-access mechanism in conformationally asymmetric trimers of the betaine transporter BetP. *Nature* 490:126–30
114. Shimamura T, Weyand S, Beckstein O, Rutherford NG, Hadden JM, et al. 2010. Molecular basis of alternating access membrane transport by the sodium-hydantoin transporter Mhp1. *Science* 328:470–73
115. Watanabe A, Choe S, Chaptal V, Rosenberg JM, Wright EM, et al. 2010. The mechanism of sodium and substrate release from the binding pocket of vSGLT. *Nature* 468:988–91
116. Krishnamurthy H, Gouaux E. 2012. X-ray structures of LeuT in substrate-free outward-open and apo inward-open states. *Nature* 481:469–74
117. Singh SK, Piscitelli CL, Yamashita A, Gouaux E. 2008. A competitive inhibitor traps LeuT in an open-to-out conformation. *Science* 322:1655–61
118. Pedersen AV, Andreassen TF, Loland CJ. 2014. A conserved salt bridge between transmembrane segments 1 and 10 constitutes an extracellular gate in the dopamine transporter. *J. Biol. Chem.* 289:35003–14
119. Kniazeff J, Shi L, Loland CJ, Javitch JA, Weinstein H, Gether U. 2008. An intracellular interaction network regulates conformational transitions in the dopamine transporter. *J. Biol. Chem.* 283:17691–701
120. Shi L, Quick M, Zhao Y, Weinstein H, Javitch JA. 2008. The mechanism of a neurotransmitter:sodium symporter-inward release of Na⁺ and substrate is triggered by substrate in a second binding site. *Mol. Cell* 30:667–77
121. Malinauskaite L, Quick M, Reinhard L, Lyons JA, Yano H, et al. 2014. A mechanism for intracellular release of Na⁺ by neurotransmitter/sodium symporters. *Nat. Struct. Mol. Biol.* 21:1006–12
122. Simmons KJ, Jackson SM, Brueckner F, Patching SG, Beckstein O, et al. 2014. Molecular mechanism of ligand recognition by membrane transport protein, Mhp1. *EMBO J.* 33:1831–44
123. Nyola A, Karpowich NK, Zhen J, Marden J, Reith ME, Wang D-N. 2010. Substrate and drug binding sites in LeuT. *Curr. Opin. Struct. Biol.* 20:415–22

124. Liao J, Li H, Zeng W, Sauer DB, Belmares R, Jiang Y. 2012. Structural insight into the ion-exchange mechanism of the sodium/calcium exchanger. *Science* 335:686–90
125. Waight AB, Pedersen BP, Schlessinger A, Bonomi M, Chau BH, et al. 2013. Structural basis for alternating access of a eukaryotic calcium/proton exchanger. *Nature* 499:107–10
- 125a. Wu M, Tong S, Waltersperger S, Diederichs K, Wang M, Zheng L. 2013. Crystal structure of $\text{Ca}^{2+}/\text{H}^{+}$ antiporter protein YfkE reveals the mechanisms of Ca^{2+} efflux and its pH regulation. *PNAS* 110:11367–72
126. Lu F, Li S, Jiang Y, Jiang J, Fan H, et al. 2011. Structure and mechanism of the uracil transporter UraA. *Nature* 472:243–46
127. Geertsma ER, Chang Y-N, Shaik FR, Neldner Y, Pardon E, et al. 2015. Structure of a prokaryotic fumarate transporter reveals the architecture of the SLC26 family. *Nat. Struct. Mol. Biol.* 22:803–8
128. Fluman N, Ryan CM, Whitelegge JP, Bibi E. 2012. Dissection of mechanistic principles of a secondary multidrug efflux protein. *Mol. Cell* 47:777–87
129. Tirosh O, Sigal N, Gelman A, Sahar N, Fluman N, et al. 2012. Manipulating the drug/proton antiporter stoichiometry of the secondary multidrug transporter MdfA. *PNAS* 109:12473–78
130. Parker JL, Mindell JA, Newstead S. 2014. Thermodynamic evidence for a dual transport mechanism in a POT peptide transporter. *eLife* 3:e04273
131. Deleted in proof
132. Boudker O, Ryan RM, Yernool D, Shimamoto K, Gouaux E. 2007. Coupling substrate and ion binding to extracellular gate of a sodium-dependent aspartate transporter. *Nature* 445:387–93
133. Yernool D, Boudker O, Jin Y, Gouaux E. 2004. Structure of a glutamate transporter homologue from *Pyrococcus horikoshii*. *Nature* 431:811–18
134. Georgieva ER, Borbat PP, Ginter C, Freed JH, Boudker O. 2013. Conformational ensemble of the sodium-coupled aspartate transporter. *Nat. Struct. Mol. Biol.* 20:215–21
135. Hanelt I, Wunnicke D, Bordignon E, Steinhoff HJ, Slotboom DJ. 2013. Conformational heterogeneity of the aspartate transporter Glt_{pH} . *Nat. Struct. Mol. Biol.* 20:210–14
136. Erkens GB, Hanelt I, Goudsmits JM, Slotboom DJ, van Oijen AM. 2013. Unsynchronised subunit motion in single trimeric sodium-coupled aspartate transporters. *Nature* 502:119–23
137. Akyuz N, Altman RB, Blanchard SC, Boudker O. 2013. Transport dynamics in a glutamate transporter homologue. *Nature* 502:114–18
138. Akyuz N, Georgieva ER, Zhou Z, Stolzenberg S, Cuendet MA, et al. 2015. Transport domain unlocking sets the uptake rate of an aspartate transporter. *Nature* 518:68–73
139. Crisman TJ, Qu S, Kanner BI, Forrest LR. 2009. Inward-facing conformation of glutamate transporters as revealed by their inverted-topology structural repeats. *PNAS* 106:20752–57
140. Kühlbrandt W, Davies KM. 2016. Rotary ATPases: a new twist to an ancient machine. *Trends Biochem. Sci.* 41:106–16
141. Morales-Rios E, Montgomery MG, Leslie AGW, Walker JE. 2015. Structure of ATP synthase from *Paracoccus denitrificans* determined by X-ray crystallography at 4.0 Å resolution. *PNAS* 112:13231–36
142. Hunte C, Screpanti E, Venturi M, Rimon A, Padan E, Michel H. 2005. Structure of a $\text{Na}^{+}/\text{H}^{+}$ antiporter and insights into mechanism of action and regulation by pH. *Nature* 435:1197–202
143. Hu N-J, Iwata S, Cameron AD, Drew D. 2011. Crystal structure of a bacterial homologue of the bile acid sodium symporter ASBT. *Nature* 478:408–11
144. Zhou X, Levin EJ, Pan Y, McCoy JG, Sharma R, et al. 2014. Structural basis of the alternating-access mechanism in a bile acid transporter. *Nature* 505:569–73
145. Wöhlert D, Kühlbrandt W, Yildiz Ö. 2014. Structure and substrate ion binding in the sodium/proton antiporter PaNhaP. *eLife* 3:e03579
146. Paulino C, Wöhlert D, Kapotova E, Yildiz Ö, Kühlbrandt W. 2014. Structure and transport mechanism of the sodium/proton antiporter MjNhaP1. *eLife* 3:e03583
147. Lee C, Yashiro S, Dotson DL, Uzdavinys P, Iwata S, et al. 2014. Crystal structure of the sodium-proton antiporter NhaA dimer and new mechanistic insights. *J. Gen. Physiol.* 144:529–44
148. Coincon M, Uzdavinys P, Nji E, Dotson DL, Winkelmann I, et al. 2016. Crystal structures reveal the molecular basis of ion translocation in sodium/proton antiporters. *Nat. Struct. Mol. Biol.* 23:248–55

149. Williams KA. 2000. Three-dimensional structure of the ion-coupled transport protein NhaA. *Nature* 403:112–15
150. Paulino C, Kuhlbrandt W. 2014. pH- and sodium-induced changes in a sodium/proton antiporter. *eLife* 3:e01412
151. Rimon A, Tzuberly T, Padan E. 2007. Monomers of the NhaA Na⁺/H⁺ antiporter of *Escherichia coli* are fully functional yet dimers are beneficial under extreme stress conditions at alkaline pH in the presence of Na⁺ or Li⁺. *J. Biol. Chem.* 282:26810–21
152. Vergara-Jaque A, Fenollar-Ferrer C, Mulligan C, Mindell JA, Forrest LR. 2015. Family resemblances: a common fold for some dimeric ion-coupled secondary transporters. *J. Gen. Physiol.* 146:423–34
153. Focke PJ, Moenne-Loccoz P, Larsson HP. 2011. Opposite movement of the external gate of a glutamate transporter homolog upon binding cotransported sodium compared with substrate. *J. Neurosci.* 31:6255–62
154. Verdon G, Oh S, Serio RN, Boudker O. 2014. Coupled ion binding and structural transitions along the transport cycle of glutamate transporters. *eLife* 3:e02283
155. Huang Z, Tajkhorshid E. 2008. Dynamics of the extracellular gate and ion-substrate coupling in the glutamate transporter. *Biophys. J.* 95:2292–2300
156. Shrivastava IH, Jiang J, Amara SG, Bahar I. 2008. Time-resolved mechanism of extracellular gate opening and substrate binding in a glutamate transporter. *J. Biol. Chem.* 283:28680–90
157. Jensen S, Guskov A, Rempel S, Hanelt I, Slotboom DJ. 2013. Crystal structure of a substrate-free aspartate transporter. *Nat. Struct. Mol. Biol.* 20:1224–26
158. Ryan RM, Compton EL, Mindell JA. 2009. Functional characterization of a Na⁺-dependent aspartate transporter from *Pyrococcus horikoshii*. *J. Biol. Chem.* 284:17540–48
- 158a. Groeneveld M, Slotboom DJ. 2010. Na⁺: aspartate coupling stoichiometry in the glutamate transporter homologue GltPh. *Biochemistry* 49:3511–13
159. Reyes N, Oh S, Boudker O. 2013. Binding thermodynamics of a glutamate transporter homolog. *Nat. Struct. Mol. Biol.* 20:634–40
160. Zhao Y, Terry D, Shi L, Weinstein H, Blanchard SC, Javitch JA. 2010. Single-molecule dynamics of gating in a neurotransmitter transporter homologue. *Nature* 465:188–93
161. Zhao Y, Terry DS, Shi L, Quick M, Weinstein H, et al. 2011. Substrate-modulated gating dynamics in a Na⁺-coupled neurotransmitter transporter homologue. *Nature* 474:109–13
162. Zhou Y, Wang X, Tzingounis AV, Danbolt NC, Larsson HP. 2014. EAAT2 (GLT-1; slc1a2) glutamate transporters reconstituted in liposomes argues against heteroexchange being substantially faster than net uptake. *J. Neurosci.* 34:13472–85
163. Pebay-Peyroula E, Dahout-Gonzalez C, Kahn R, Trezeguet V, Lauquin GJ, Brandolin G. 2003. Structure of mitochondrial ADP/ATP carrier in complex with carboxyatractyloside. *Nature* 426:39–44
164. Verdon G, Boudker O. 2012. Crystal structure of an asymmetric trimer of a bacterial glutamate transporter homolog. *Nat. Struct. Mol. Biol.* 19:355–7